Cytonuclear discordance and historical demography of two brown frogs, Rana tagoi and R. sakuraii (Amphibia: Ranidae).

AUTHOR(S):

Eto, Koshiro; Matsui, Masafumi

CITATION:

Eto, Koshiro ...[et al]. Cytonuclear discordance and historical demography of two brown frogs, Rana tagoi and R. sakuraii (Amphibia: Ranidae).. Molecular phylogenetics and evolution 2014, 79C: 231-239

ISSUE DATE:

2014-06-27

URL:

http://hdl.handle.net/2433/189320

Cytonuclear Discordance and Historical Demography of Two Brown Frogs, *Rana tagoi* and *R. sakuraii* (Amphibia: Ranidae)

KOSHIRO ETO and MASAFUMI MATSUI*

Graduate School of Human and Environmental Studies, Kyoto University, Yoshida Nihonmatsu-cho, Sakyoku, Kyoto 606-8501, Japan

*Corresponding author. Phone: +81-75-753-6846;
FAX: +81-75-753-6846;
E-mail: fumi@zoo.zool.kyoto-u.ac.jp

Abstract

Prior studies of mitochondrial genomic variation reveal that the Japanese brown frog *Rana tagoi* comprises a complex of cryptic species lineages, and that *R. sakuraii* arose from within this complex. Neither species forms a monophyletic group on the mitochondrial haplotype tree, precluding a simple explanation for the evolutionary origins of *R. sakuraii*. We present a more complete sampling of mitochondrial haplotypic variation (from the *ND1* and *16S* genes) plus DNA sequence variation for five nuclear loci (from the genes encoding *NCX1*, *NFIA*, *POMC*, *SLC8A3*, and *TYR*) to resolve the evolutionary histories of these species. We test hypotheses of population assignment (STRUCTURE) and isolation-with-migration (IM) using the more slowly evolving nuclear markers. These demographic analyses of nuclear genetic variation confirm species-level distinctness and integrity of *R. sakuraii* despite its apparent polyphyly on the mitochondrial haplotype tree. Divergence-time estimates from both the mitochondrial haplotypes and nuclear genomic markers suggest that *R. sakuraii* originated approximately one million years ago, and that incomplete sorting of mitochondrial haplotype lineages best explains

non-monophyly of *R. sakuraii* mitochondrial haplotypes. Cytonuclear discordance elsewhere in *R. tagoi* reveals a case of mitochondrial introgression between two species lineages on Honshu. The earliest phylogenetic divergence within this species group occurred approximately four million years ago, followed by cladogenetic events in the Pliocene and early Pleistocene yielding 10–13 extant species lineages, including *R. sakuraii* as one of the youngest.

Key words: species complex; incomplete lineage sorting; introgression; isolation with migration

1. Introduction

Japanese brown frogs *Rana tagoi* and *R. sakuraii* are known to show a complicated genealogical relationship (Tanaka et al., 1996; Eto et al., 2012, 2013). *Rana tagoi* occurs widely on the main and peripheral islands of the Japanese archipelago except for Hokkaido and the Ryukyus. While most brown frogs breed in open, still waters, *R. tagoi* breeds in subterranean streams where the larvae can metamorphose without feeding (Matsui and Matsui, 1990; Maeda and Matsui, 1999). These distinctive traits might be the product of adaptation to the mountainous environments of the Japanese archipelago. Conversely, *R. sakuraii*, occurring only on Honshu sympatric with *R. tagoi*, breeds under rocks in open streams, and adult frogs have several characters suitable for a lotic environment (e.g., they possess fully developed toe webs, which are less well developed in *R. tagoi*), although its eggs and larvae share traits with those of *R. tagoi*. From these facts, Matsui and Matsui (1990) postulated that *R. sakuraii* speciated from a *R. tagoi*-like ancestor when it adapted to stream environments. This hypothesis is supported by phylogenetic analyses of mitochondrial haplotypes, in which *R. sakuraii* is embedded in *R. tagoi* lineages (Tanaka et al., 1996; Eto et al., 2012). However, neither of the species is monophyletic on the mitochondrial haplotype tree (Eto et al., 2012). Mitochondrial haplotype variation reveals that *R. tagoi* is divided into numerous species lineages, and some of these lineages are reproductively isolated from each other (Eto et al., 2012, 2013). As is clear from

these studies, *R. tagoi* contains multiple cryptic species, one of which is the sister taxon to *R. sakuraii*. Two hypotheses potentially explain polyphyly of *R. sakuraii* haplotypes on the mitochondrial haplotype phylogeny. Incomplete lineage sorting (ILS), retention of disparate haplotype lineages from an *R. tagoi*-like ancestor, is the simplest explanation if *R. sakuraii* originated very recently, within the past approximately one million years. Alternatively, introgression of mitochondrial haplotypes resulting from gene flow between *R. sakuraii* and a sympatric lineage of *R. tagoi* could explain the anomalous phylogenetic distribution of *R. sakuraii* mitochondrial haplotypes.

In this study, we analyse sequence data for two mitochondrial and five nuclear loci to test these hypothesis and to estimate divergence times and demographic patterns of these two species. Expanded sampling of mitochondrial haplotype variation relative to earlier studies yields increased precision of the mitochondrial phylogenetic analysis. We test hypotheses of population assignment (Pritchard et al, 2000) and isolation-with-migration (IM; Hey, 2010) using the more slowly evolving nuclear markers to verify inferences made from the mitochondrial haplotype phylogeny.

2. Materials and Methods

2.1. Sampling strategy

For each species, we chose samples belonging to representative localities/mt-lineages based on previous studies (e.g., Eto et al., 2012). We analysed 107 samples of *R. tagoi* (including three samples each of the subspecies *R. t. yakushimensis* and *R. t. okiensis* from peripheral islands) and 21 of *R. sakuraii* from 81 localities (Fig. 1, Table S1). To the mtDNA phylogenetic analysis, we added GenBank data for *R. kobai* (AB685768), *R. sauteri* (AB685767), *R. tsushimensis* (AB639592, AB639752), and *R. ulma* (AB685780) as outgroup taxa based on known phylogenetic relationships (Tanaka-Ueno et al., 1996, 1998).

79 *2.2. Sequencing of DNA*

80 Total DNA was extracted from frozen or ethanol-preserved tissues using standard phenol-
81 chloroform extraction procedures. Then, we amplified fragments containing the target region
82 (two mitochondrial genes, 16S ribosomal RNA [*16S*] and NADH dehydrogenase subunit 1
83 [*ND1*]; and five nuclear genes, sodium-calcium exchanger 1 [*NCX1=SLC8A1*], nuclear factor
84 I/A [*NFIA*], pro-opiomelanocortin [*POMC*], sodium-calcium exchanger 3 [*SLC8A3*], and
85 tyrosinase [*TYR*]) by polymerase chain reaction (PCR). The experimental conditions and PCR
86 techniques were essentially identical to those reported previously (Eto et al., 2012). The
87 amplified PCR products were purified by polyethylene glycol (PEG) precipitation. The cycle
88 sequence reactions were performed out with an ABI PRISM Big Dye Terminator ver. 3.1 Cycle
89 sequencing Kit (Applied Biosystems) and sequenced on an ABI 3130 automated sequencer. We
90 used the primers listed in Table S2 for PCR and sequencing, and all samples/loci were
91 sequenced in both directions.
92
93 *2.3. Alignment of DNA, haplotype determination, and data characteristics*
94 Sequence alignment was conducted using MUSCLE (Edgar, 2004). For heterozygous
95 nuclear genes, we used PHASE ver. 2.1 (Stephens et al., 2001) to determine haplotypes. In this
96 analysis, the threshold of probability was set to small values (0.5–0.6) following Garrick et al.
97 (2010). Before analysing the historical demography, we also used IMgc (Woerner et al., 2007)
98 to detect the largest non-recombining block of nDNA for IM analysis, because IMa2 assumes
99 no intra-locus recombination (Hey and Nielsen, 2004). As data parameters, we calculated the
100 summary statistics of variable sites (*vs*), number of haplotypes (*h*), haplotype diversity (H_d), and
101 nucleotide diversity (π). We also checked the neutrality of the five nuclear loci with Tajima's *D*
102 (Tajima, 1989). Since none of them showed significant deviation from zero (Table S3), these
103 loci were considered neutral markers. We conducted all of these calculations using DnaSP
104 (Rozas et al., 2003).

105

106 *2.4. Population assignment based on mtDNA*

107 A phylogenetic analysis was conducted using the two mitochondrial genes. First, we
108 selected the best substitution model for each gene using Kakusan4 (Tanabe, 2011) based on the
109 Akaike information criterion (AIC). Then, phylogenetic trees based on the maximum-likelihood
110 method (ML) and Bayesian inference (BI) were constructed using TREEFINDER ver. Mar.
111 2011 (Jobb, 2011) and MrBayes ver. 3.2.1 (Ronquist and Huelsenbeck, 2003), respectively. For
112 the ML tree, we conducted non-parametric bootstrap analysis with 1000 replicates, and
113 branches with a bootstrap value (BS) of 70% or greater were regarded as significantly supported.
114 In the BI analysis, two independent runs of four Markov chains were conducted for 10 million
115 generations (sampling frequency one tree per 100 generations); the first three million
116 generations were discarded as burn-in. Convergence of parameters was checked using Tracer
117 ver. 1.5 (Rambaut and Drummond, 2009). We considered a Bayesian posterior probability
118 (BPP) of 0.95 or greater as significant support. From the results of both analyses, we used
119 mitochondrial haplotype clades, levels of haplotype divergence, and geographic distributions to
120 diagnose hypothetical species lineages, which were treated as population units based on mtDNA
121 in the later analyses.

122

123 *2.5. Population assignment based on nDNA*

124 *Rana tagoi* and *R. sakuraii* are so close genetically as to cause difficulty constructing
125 phylogenetic trees using nDNA sequences (Eto et al., 2012, 2013). Therefore, we conducted
126 clustering analysis using STRUCTURE ver. 2.3.3 (Pritchard et al., 2000) to delimit population
127 units based on nDNA. We applied an admixture and allele-frequency-independent model to
128 haplotype data for the nuclear loci, and calculated 500,000 generations following 100,000
129 generations of burn-in. The number of clusters (*K*) was set from 1 to 10, and 10 independent
130 iterations were conducted for each *K*. The most likely *K* was determined by the likelihood

distribution of each iteration and the delta *K* value (Evanno et al., 2005). We also constructed haplotype networks for each gene based on the median-joining method using Network ver. 4.6 (Bandelt et al., 1999) to examine the relationships among nuclear haplotypes.

2.6. Divergence dating based on mtDNA

To estimate the divergence time between mt-lineages, we conducted Bayesian analysis using BEAST ver. 1.7.5 (Drummond et al., 2012). For each calibration, 10 million generations of run (of which the first three million were discarded as burn-in) were conducted under a non-autocorrelated log-normal relaxed clock model. Tracer ver. 1.5 (Rambaut and Drummond, 2009) was used to check the parameter distributions and effective sample size. We applied the following two different calibrations:

Calibration I: The molecular evolutionary rate of 1.38% (0.69% per lineage) per MY was applied. This value was estimated for the *ND1* and *ND2* regions of *Bufo* (Macey et al., 1998), and only *ND1* data were used in this calculation. The evolutionary rate of this region is similar among a wide range of vertebrates (Macey et al., 2001). We thus used that rate, despite considerable phylogenetic distance between *Rana* and *Bufo*.

Calibration II: Using only *16S* data, we applied the evolutionary rate of 0.66% (0.33% per lineage) per MY estimated for *16S* of *Leiopelma* (Fouquet et al., 2009).

2.7. Estimation of historical demography

The historical demography, especially the patterns of gene flow and divergence times among species or genetic groups, was examined using coalescent analysis with the Bayesian IM model. We analysed the nDNA data using the program IMa2 (Hey 2010), and estimated the effective population size, N_e, population migration rate, $2N_eM$, and population divergence time, *T*. As the mutation rate of nuclear genes, we applied 0.047% per MY per lineage for *NCX1* (reported in the genus *Hydromantes*; Rovito 2010), 0.072% (0.061–0.083%) for *POMC*

(*Hyperolius*; Lawson, 2010), and 0.047% (0.027–0.067%) for *SLC8A3* (amphibians in general; Roelants et al., 2007). The geometric mean of these values, approximately 2.71×10^{-7} mutations per year per locus, was used as the mutation rate (μ) to scale each demographic parameter. Based on several test runs, the upper bounds for the parameters were set at θ = 10–20, t = 3–5, and m = 10–25, and five million steps (sampling frequency one tree per 50 steps) of calculations were performed for 30 heated chains after two million burn-in steps. We conducted three independent runs, and finally combined the results using the L-mode option of IMa2. Since *R. tagoi* and *R. sakuraii* typically start to breed at the age of 3 years (Kusano et al., 1995a, b), we applied this value as the generation time of the two species. The trendline plots and effective sample sizes were monitored to ensure good mixing and convergence of parameters.

The significance of $2N_eM$ was determined using the log-likelihood ratio (LLR) test of Nielsen and Wakeley (2001). We also used the parameter comparison option (with the -p6 command) of IMa2 and output the list of probability, which indicates one parameter to be greater than the other. The relative strength of genetic isolation was evaluated using $2N_eM$ values (strong [$2N_eM \leq 1$], moderate [$1 < 2N_eM \leq 5$], and weak [$5 < 2N_eM \leq 25$]: Wright, 1931; Waples and Gaggiotti, 2006; Reilly et al., 2012).

3. Results

3.1. Sequence characteristics

We obtained complete mitochondrial *16S* (1612bp) and *ND1* (967bp) sequences for all samples. There were 489 parsimoniously informative sites within the ingroup: 244 for *16S* and 245 for *ND1*. The other statistics are listed in Table S3.

In the sequences of the five nuclear loci for all 128 samples, only *POMC* had in-dels, and these sites were omitted from the subsequent analyses. For haplotype determination using PHASE, all haplotypes in all samples/loci were determined successfully, except for one sample for *POMC* and two for *TYR*, which were treated as null alleles in subsequent analyses. The

sequence length and statistics of each locus are listed in Table S3. Overall, each parameter generally indicated great genetic diversity in *R. tagoi* and *R. sakuraii*. Of the five nuclear loci, *TYR* was the most variable (H_d = 0.955 and π = 0.017 for all samples) and *NFIA* was the least variable (0.735 and 0.003, respectively).

3.2. Population assignment: Mitochondrial DNA results

The best substitution model selected in the ML analysis was the general time reversible (GTR; Tavaré, 1986) model with the optimized gamma shape parameter (G) of 0.158 and the proposition of invariable sites (I) of 0.144 for *16S* and the J1 (Jobb, 2011) model + G (0.543) + I (0.312) for *ND1*. For BI, the models were GTR + G (0.082) + I (0.226) and GTR + G (0.892) + I (0.226) for *16S* and *ND1*, respectively. The constructed ML (–ln*L* = 15500.618) and BI (15863.190) trees were essentially identical in topology, and only the ML tree is shown in Fig. 2. We followed Eto et al. (2012) for the names of each genetic group.

The phylogenetic relationships obtained were fundamentally identical to those reported by Eto et al. (2012). The ingroup was divided into two large haplotype clades (A and B), and both of these included subclades judged by their geographic distributions to diagnose separate species lineages (A-1ab to A-9abc and B-1 to B-2ab); Clade B (ML-BS = 82% and BPP = 1.00) contained only haplotypes from *R. tagoi*, while Clade A (ML-BS = 93% and BPP = 1.00) included both *R. tagoi* and *R. sakuraii* haplotypes. Each clade/lineage was well supported (ML-BS≧70%, BPP≧0.95). The statistical support for nodes was generally better than in the previous study, and more detailed phylogenetic relationships were clarified, particularly those among the lineages in Clade A. In Clade A, the lineages from Honshu Island (A-1ab to A-6) formed a subclade (A' in Fig. 2. ML-BS = 73% and BPP = 0.98) against the Shikoku and Kyushu subclade (A''; ML-BS = 79% and BPP = 0.95). Within Subclade A', three additional lineage groups were recognised: one consisted of Lineages A-1a and A-1b (ML-BS = 82% and BPP = 1.00); the second of Lineages A-2 and A-3 (ML-BS = 70% and

BPP = 0.98); and the third Lineages A-4, A-5, and A-6 (ML-BS = 79% and BPP = 1.00). The haplotypes obtained from *R. sakuraii* were included in Lineages A-2 and A-3. Lineage A-2 also contained *R. tagoi* haplotypes, although haplotypes were not shared between the two species.

3.3. Population assignment: Nuclear DNA results

The results of the clustering analysis using STRUCTURE are shown in Fig. 3. For all samples, $K = 2$ was supported by the test of delta K, and two clusters (I and II) were recognised. Almost all samples were clearly assigned to each cluster (posterior probabilities ≥ 80%), indicating strong genetic isolation between the two nDNA clusters. Although the division of the two nuclear clusters (I and II) did not completely correspond to that of the two mitochondrial clades (A and B), Cluster II was largely concordant with mitochondrial Subclade A', with the exception of Lineage A-1a (Fig. 3). Clusters I and II also were separated on the haplotype networks of some nuclear genes (e.g., *NCX1*, *NFIA*, and *SLC8A3*; Fig. S1). However, in relatively more variable genes like *TYR*, the haplotype relationships were highly complex and their separation was not clear (Fig. S1). Furthermore, haplotypes were more or less shared between Clusters I and II in all loci, indicating ILS in these nuclear genes.

Since the two large clusters seemed to contain several subclusters, we independently reanalysed samples for the two clusters. Within Cluster I, the population assignment with $K = 2$ was supported (Fig. 3). In this clustering, the division of subclusters was still roughly correlated with the mt-lineages: the lineages from the main islands (A-1a, A-7, A-9a, and B-2ab) tended to form a subcluster and the lineages from the peripheral islands (A-8, A-9c, and B-1) formed another. One lineage, A-9b, included samples assigned to both of these subclusters. Except for Lineage A-9b, samples of the two subclusters were clearly assigned to either subcluster. In contrast, $K = 3$ was supported within Cluster II using the delta K test and likelihood distribution. In this division, *R. tagoi* Lineages A-1b and A-4, *R. tagoi* A-2, and *R. sakuraii* (A-3 and part of A-2) each formed a subcluster (Fig. 3). The separation of these subclusters was clear (posterior

probabilities > 80%), with a few exceptional samples in the *R. sakuraii* subcluster. By contrast, many samples of lineages A-5 and A-6 were not clearly assigned to particular subclusters, and showed intermediate genetic structures between *R. tagoi* of A-2 and *R. sakuraii*.

3.4. Divergence times of the mitochondrial lineages

The results of divergence dating for the major nodes on the mitochondrial genealogy are listed in Table 1. Although we applied the evolutionary rates of phylogenetically remote taxa (*Bufo* and *Leiopelma*) the divergence times obtained for the ingroup were similar in the two calibrations. Two major mt-clades (A and B: node 1 in Fig. 2) were estimated to have diverged 4.2–4.0 (95% highest posterior density interval [HPD] of 6.2–2.3) MYA. Then Subclades A' and A" (node 2) split 2.8–2.6 (4.1–1.6) MYA, followed by the separation within Clade B (node 22) 2.7–2.3 (4.3–1.2) MYA. The two lineages including *R. sakuraii* samples, A-2 and A-3, separated from each other 2.1–1.9 (3.1–1.1) MYA (node 7), followed by internal divergence during 1.4–0.9 (2.2–0.4) MYA (nodes 8 and 9). The most recently divergent lineages were B-2a and B-2b (node 23), which split at 1.4 (2.2–0.7) MYA. These estimates indicate that the divergence of each major mitochondrial clade/lineage began in the mid-to-late Pliocene and was approaching completion in the mid Pleistocene.

3.5. Historical demography

As shown above, the results of the population assignment were not completely concordant between mt- and n-DNA (Figs. 2 and 3). In estimating demographic parameters, we used only nDNA data because nuclear markers are thought to be more conservative than mitochondrial ones, which are more likely to be affected by introgression than the nuclear markers (Ballard and Whitlock 2004).

3.5.1. Historical demography between Clusters I and II

First, we conducted a coalescent analysis using IMa2 for the two large nuclear clusters: I and II. Each parameter showed single peaks in their probability density distributions (Fig. S2). The parameter values obtained are listed in Table 2. The estimated population migration rate ($2N_eM$) for I to II (I → II) was 0.52 (0.24–1.12). In the opposite direction; *i.e.* II → I, the parameter value tended to be larger, with $2N_eM_{\mathrm{II}\rightarrow\mathrm{I}}$ being 1.23 (0.70–2.14). The LLR test showed that all of these values were significantly larger than zero ($p < 0.01$), suggesting that clusters I and II have maintained a degree of gene flow after their divergence. However, strong to moderate genetic isolation would exist between the two clusters because the $2N_eM$ values obtained were relatively small (ca. 1 or smaller: Wright, 1931; Waples and Gaggiotti, 2006; Reilly et al., 2012). The effective population size estimated for I, II, and their ancestor was 2.2 (1.7–2.9), 1.7 (1.3–2.3), and 0.4 (0.2–0.8) million individuals, respectively. The ancestral population size was smaller than those at present, as supported by parameter comparison of θ (the posterior probabilities were 1.00 for each comparison). The population size of II tended to be smaller than that of I, but the tendency was not supported statistically (BPP < 0.95). The population divergence time (T) of I and II was estimated as 2.7 (4.4–2.2) MYA. Although its 95%HPD was relatively wide, this estimate was younger than the divergence time of the two major mt-clades (A/B; ca. 4.2–4.0 MYA), but almost equal to those of A'/A" (ca. 2.8–2.6 MYA) and B-1/B-2 (ca. 2.7–2.3 MYA) (Table 1).

3.5.2. Historical demography between R. tagoi *and* R. sakuraii

Then, we compared demographic parameters between *R. tagoi* and *R. sakuraii*. As *R. tagoi* (*Rt*), we chose mt-Lineages A-2, 5, and 6, which were genetically close to *R. sakuraii* (*Rs*) in the mitochondrial and nuclear DNA analyses, as shown above (see Figs. 2 and 3). Since our dataset was not sufficiently informative to analyse a four-populations model, we combined Lineages A-5 and A-6 as a single group; these showed close genetic relationships in both

mitochondrial and nuclear analyses (Figs. 2, 3). We conducted two separate analyses under different population schemes: (1) three-populations model, in which *R. sakuraii* (*Rs*) and *R. tagoi* (*Rt*) Lineage A-2 were assumed to be mutually close compared to A-5 and 6, based on the mtDNA genealogy, and (2) two-populations model based on the current classification (*Rs* vs. *Rt* A-2, 5, and 6).

In the three-populations model, significant gene flow ($p < 0.05$ in the LLR test) was detected only in *R. tagoi* A-5+6 → A-2 ($2N_eM_{Rt\ A\text{-}5+6 \rightarrow Rt\ A\text{-}2}$ was 3.79 [0.75–9.50]; Fig. S3 and Table 2) and A-5+6 → *R. sakuraii* ($2N_eM_{Rt\ A\text{-}5+6 \rightarrow Rs}$ was 0.40 [0.04–2.00]), and no significant gene flow was recognized between *R. sakuraii* and *R. tagoi* A-2 ($p > 0.05$). These results indicated that the genetic isolation between *R. tagoi* A-2 and A-5+6 was moderate ($1 < 2N_eM \leq 5$), but the gene flow was strongly biased to one direction (from A-5+6 to A-2). Although gene flow existed between the two species, the direction was limited (*R. tagoi* A-5+6 → *R. sakuraii*), and the population migration rate obtained was small ($2N_eM \leq 1$), indicating strong genetic isolation between *R. sakuraii* and *R. tagoi* lineages. The estimated effective population size (a million individuals) was similar between *R. tagoi* A-2 (0.80 [0.34–2.06]) and A-5+6 (0.79 [0.38–1.76]), but was smaller in *R. sakuraii* (0.16 [0.07–0.32]). This tendency was supported in the statistical test, in which N_e for *R. sakuraii* was significantly smaller than those for *R. tagoi* lineages (BPP > 0.95).

We could not obtain a sufficient estimate for gene flow between the ancestral populations because no obvious peaks of probability for the parameter $2N_eM$ were recognised (Table 2). The estimated ancestral population size (N_e) was 0.21 (0.01–4.06) for *R. sakuraii* + *R. tagoi* A-2, and was 0.43 (0.23–0.77) for the common ancestor of *R. sakuraii*, *R. tagoi* A-2 and A-5+6. The estimated N_e for the ancestors tended to be smaller than the present N_e for *R. tagoi* (A-2, A-5+6) and larger than that for *R. sakuraii*, but the tendencies were not supported statistically (BPP < 0.95). The time of population divergence estimated for *R. sakuraii*/*R. tagoi* A-2 (1.1 [2.3–0.6]

MYA) was much younger than that for the ancestors (2.15 [6.11–1.31] MYA), although the credibility intervals largely overlapped.

In the two-populations model, significant gene flow from *R. tagoi* to *R. sakuraii* was again detected ($2N_eM_{Rt \rightarrow Rs}$ was 0.51 [0.14–1.17]: Fig. S3 and Table 2), but such trend was not recognized in the opposite direction (Fig. S3 and Table 2). These results indicate strong to medium isolation between the two species, although small and unidirectional gene flow exists. The $2N_eM$ value for *R. tagoi* → *R. sakuraii* in this model was similar to the value for *R. tagoi* A-5+6 → *R. sakuraii* in the three-populations model shown above (Table 2).

The estimated N_e showed values and tendencies similar to those obtained in the three-populations model; N_e for *R. sakuraii* (0.17 [0.09–0.34]) was significantly smaller (BPP > 0.95) than that of *R. tagoi* (1.61 [0.99–2.65]). The estimates for ancestral N_e (0.37 [0.10–0.68] in the two-populations model) also are similar between the models. The divergence time estimated for the two species, 1.2 (2.9–0.6) MYA, was slightly older than that estimated by the three-population model (ca. 1.1 MYA).

4. Discussion

4.1. Discordance between the classification and patterns of genetic variation using different markers

Our new data and analyses confirmed the major patterns of mitochondrial genomic variation reported previously (Eto et al., 2012). Mitochondrial haplotypes obtained from *R. sakuraii* were genealogically embedded in those from *R. tagoi*, and neither species was monophyletic on the haplotype tree. The mitochondrial and nuclear data considered together indicate that *R. sakuraii* constitutes a single species lineage. *Rana sakuraii* corresponds largely to Lineage A-3 on the mitochondrial haplotype tree (Fig. 2), with its sister lineage being *R. tagoi* populations bearing mitochondrial haplotypes of Lineage A-2. Nonetheless, Lineage A-2 includes some *R. sakuraii*

337 mitochondrial haplotypes. We examine the hypotheses of incomplete lineage sorting and gene
338 flow as possible explanations for this pattern. The following three scenarios could explain the
339 phylogenetic pattern of mitochondrial haplotypes of lineages A-2 and A-3 (Fig. 2): (1) recent
340 speciation of *R. sakuraii* from *R. tagoi* Lineage A-2, which led to ILS of mtDNA at the species
341 level; (2a) past mitochondrial introgression from *R. tagoi* A-2 to *R. sakuraii*; and (2b)
342 introgression in the opposite direction (Fig. 4). If recent separation of *R. sakuraii* from *R. tagoi*
343 A-2 was the case, the ILS hypothesis (1) would be the simplest explanation. However, if the
344 speciation was shown to be old, especially much older than the divergence time within mt-
345 Lineage A-2, this hypothesis would be rejected. Conversely, the past-introgression hypotheses
346 (2) would be applicable if the speciation of the two species coincided with the split between
347 Lineages A-2 and A-3 (2a), or the separation of these two lineages from the others (2b).
348 Detection of historical gene flow between *R. sakuraii* and *R. tagoi* A-2 for the nuclear markers
349 also would support the past introgression hypotheses.

350 The genetic relationship based on the STRUCTURE analysis using nDNA was discordant
351 with the mitochondrial genealogy, and *R. sakuraii* and *R. tagoi* A-2 tended to be separated in
352 different subclusters (Fig. 3). This result likely reflects their heterospecific status. The
353 demographic analysis using IMa2 showed that the separation of *R. sakuraii* from *R. tagoi*
354 lineages (ca. 1.1 MYA and 1.2 MYA in three- and two-populations models, respectively; Table
355 2) was younger than the separation of mt-Lineages A-2 and A-3 (ca. 2.1–1.9 MYA; Table 1),
356 and was similar to the divergence within these lineages (ca. 1.4–0.9 MYA). The date of
357 speciation would correspond to, or be younger than, the population divergence time estimated
358 by IMa in this case. So these results favour the ILS hypothesis, although the credibility intervals
359 of these estimates overlapped.

360 Based on the genealogy obtained (Fig. 2), mitochondrial introgression between *R. tagoi* A-2
361 and *R. sakuraii* happened several times if the hypotheses 2 were the case (for example, two
362 independent introgression events should be presumed in the hypothesis 2a). Thus the

introgression hypotheses assume rampant hybridization of *R. tagoi* A-2 and *R. sakuraii* in the past. The IM analyses based on two different models showed gene flow from *R. tagoi* to *R. sakuraii*. However, this unidirectional gene flow seems to depend largely on the flow from *R. tagoi* A-5+6 to *R. sakuraii*, because no significant flow between *R. tagoi* A-2 and *R. sakuraii* was detected (Table 2). These results do not support rampant hybridization of *R. tagoi* A-2 and *R. sakuraii*, even though inter-specific gene flow did exist. From these considerations, the ILS hypothesis would be more plausible than the introgression hypothesis to explain the relationships of the two species on the mitochondrial genealogy.

The estimated time of the split of *R. sakuraii* and *R. tagoi* Lineage A-2 (ca. 1.2–1.1 MYA) is younger than those of other Japanese frogs (e.g., ca. 2.3 MYA between *Odorrana ishikawae*/*O. splendida* and ca. 1.7 MYA between *O. amamiensis*/*O. narina* [Matsui et al., 2005]; and around 5.7–4.0 MYA among *Bufo torrenticola* and two subspecies of *B. japonicus* [Igawa et al., 2006]), and seems to have occurred after the rough formation of the Japanese archipelago (see the next section). Although the ILS of mtDNA at the species level is relatively rare because of its small effective number of gene copies, it occurs occasionally in some situations, such as speciation within the past millions years. It could be applicable in the case of *R. sakuraii* and *R. tagoi*, because their speciation is estimated to be only about one million year ago. *Rana sakuraii* has several traits adaptive to stream breeding in contrast to the subterranean breeding *R. tagoi*, although they share many other characters (Matsui and Matsui, 1990). It suggests that the speciation of *R. sakuraii* was triggered by adaptation to a new breeding habitat, which is a process that often promotes rapid speciation (Coyne and Orr, 2004).

4.2. Evolutionary history of the two species

Rana tagoi and *R. sakuraii* are endemic to the Japanese archipelago and no close relatives are known from the continent, although *R. sauteri*, a lotic breeding brown frog from Taiwan, is thought to be their sister lineage (Tanaka-Ueno et al., 1998). Our data do not contradict with this idea (Fig. 1). Since the continental allies of *R. sauteri* are also unknown, the dispersal route of

the ancestor of the *R. tagoi* complex to the Japanese mainland is uncertain. The estimated time of separation of *R. sauteri* and *R. tagoi* complex varies between the calibrations (22.0–11.6 MYA; Table 1), but around the early to middle Miocene. In this period the opening of the Japan Sea began (Iijima and Tada, 1990), although the Japanese and Ryukyu archipelagos, as well as Taiwan were not yet isolated from the Eurasian continent (Chinzei and Machida, 2001). Therefore the common ancestor of *R. sauteri* and the *R. tagoi* complex would have been distributed in the continental areas corresponding to the present Japanese archipelago to Taiwan, but the ancestral allies would have been extinguished thereafter on the continent and the Ryukyus, leaving relict species in Japan and Taiwan.

In any case, the ancestral population of the *R. tagoi* complex is thought to have diverged into two major clades, A and B (Fig. 2), in the mid Pliocene (ca. 4.2–4.0 MYA). The ancient Japanese archipelago was already roughly formed by the late Miocene (Chinzei and Machida, 2001), and the separation of lineages ancestral to the clades is thought to have occurred on the archipelago. The ancestor at this period would have been a *R. tagoi*-like subterranean breeder because all of the present genetic groups of the two species have a common larval trait (e.g., no need to feed until metamorphosis) thought to be adapted to such an environment.

Then, the divergence within Clade A occurred in the late Pliocene (ca. 2.8–2.6 MYA), separating populations on or near Honshu from ones on or near from Kyushu and Shikoku. Cluster II as identified by nuclear markers (Fig. 3) is equivalent to populations diagnosed by mitochondrial haplotype Subclade A' excluding Lineage A-1a. Lineages of Subclade A' occur on Honshu, whereas those of mitochondrial Subclade A" are associated with Kyushu or Shikoku. Because populations of mitochondrial haplotype Clade B also occur on Honshu, Honshu is likely the ancestral source of this species complex, and expansion to the ancestral areas of Kyushu and Shikoku likely produced the major cladogenetic event within mitochondrial Clade A. Approximately 1.8–1.4 MYA (the divergence time estimated for mitochondrial haplotypes of Lineages A-1a and A-1b), introgression of mitochondrial haplotypes from a population in

mitochondrial Subclade A' to one in Clade B produced the anomalous result that Lineage A-1a appears in an incorrect position on the mitochondrial haplotype tree. The best interpretation is that Lineage A-1a is closest phylogenetically to the lineages of mitochondrial Clade B as revealed by the nuclear markers, in contrast to its position on the mitochondrial haplotype tree. Occurrence of Subclade A' and Clade B in geographic proximity on Honshu further supports this interpretation. The divergences within SubcladesA', A", and Clade B started around 2.7–2.3 MYA, and splitting of the major mt-lineages was roughly completed by the middle Pleistocene (around 1.4 MYA). In this period, the populations on peripheral islands were isolated geographically, and some survived and evolved into the extant subspecies; *i.e.*, *R. t. yakushimensis* of Lineage A-8 and *R. t. okiensis* of B-1.

The estimated date of speciation of *R. sakuraii* was younger than the formation of the major population lineages discussed above. *Rana sakuraii* would have originated ca. 1.2–1.1 MYA based on the IM analysis (Table 2), likely in association with the adaptation to a new breeding environment as discussed above. The effective population size of *R. sakuraii* (ca. 0.2 million individuals) is smaller than that of the closest mt-lineage of *R. tagoi* (ca. 0.8 million individuals for Lineage A-2), and suggests that a small ancestral population adapted to stream breeding led to *R. sakuraii*.

5. Conclusion

Our data reveal that *R. tagoi* comprises multiple species lineages, which form a paraphyletic group with respect to *R. sakuraii*. Because *R. sakuraii* arose only about one million years ago, incomplete lineage sorting of mitochondrial haplotypes best explains non-monophyly of *R. sakuraii* on the mitochondrial haplotype tree. Our study illustrates how mitochondrial haplotype phylogenies combined with multilocus demographic analyses of nuclear haplotypes permits precise resolution of species lineages and their genetic interactions.

Acknowledgements

We would like to thank G. Aoki, K. Araya, H. Fujita, T. Hayashi, A. Hamidy, T. Hikida, M. Kato, Y. Kawahara, K. Kawauchi, Y. Kokuryo, N. Kuraishi, N. Maeda, Mm, Matsui, T. Matsuki, T. Matsuo, Y. Misawa, Y. Miyagata, A. Mori, S. Mori, N. Nakahama, T. Nakano, Y. Nakase, K. Nishikawa, S. Okada, J. Oki, M. Sakamoto, T. Shimada, T. Sugahara, T. Sugihara, H. Takeuchi, S. Tanabe, A. Tominaga, T. Ueno, M. Yamagami, Y. Yamane, Y. Yamazaki, N. Yoshikawa, and everyone else who helped us in collecting specimens. KE thanks N. Kuraishi and N. Yoshikawa for assisting laboratory works. We are also grateful to A. Larson and anonymous reviewers for valuable comments on the manuscript. This work was partly supported by grants from the Ministry of Education, Science and Culture, Japan (Nos. 07454234, 20405013 and 23405014) to MM.

References

Ballard, J.W.O., Whitlock, M.C., 2004. The incomplete natural history of mitochondria. Mol. Ecol. 13, 729–744.

Bandelt, H., Forster, P., Röhl, A., 1999. Median-joining networks for inferring intraspecific phylogenies. Mol. Biol. Evol. 16, 37–48.

Chinzei, K., Machida, H., 2001. Formation history of structural landforms and tectonic landforms in Japan, in: Yonekura, N., Kaizuka, S., Nogami, M., Chinzei, K. (Eds.), Regional Geomorphology of the Japanese Islands, Introduction to Japanese Geomorphology, Vol. 1. University of Tokyo Press, Tokyo, pp. 298–311.

Coyne, J.A., Orr, H.A., 2004. Speciation. Sinauer Associates, Sunderland, MA.

Drummond, A.J., Suchard, M.A., Xie, D., Rambaut, A., 2012. Bayesian phylogenetics with BEAUti and the BEAST 1.7. Mol. Biol. Evol. 29, 1969–1973.

Edgar, R., 2004. MUSCLE: multiple sequence alignment with high accuracy and high throughput. Nucleic Acids Res. 32, 1792–1797.

Eto, K., Matsui, M., Sugahara, T., 2013. Discordance between mitochondrial DNA genealogy and nuclear DNA genetic structure in the two morphotypes of *Rana tagoi tagoi* (Amphibia: Anura: Ranidae) in the Kinki Region, Japan. Zool. Sci. 30, 553–558.

Eto, K., Matsui, M., Sugahara, T., Tanaka-Ueno, T., 2012. Highly complex mitochondrial DNA genealogy in an endemic Japanese subterranean breeding brown frog *Rana tagoi* (Amphibia, Anura, Ranidae). Zool. Sci. 29, 662–671.

Evanno, G., Regnaut, S., Goudet, J., 2005. Detecting the number of clusters of individuals using the software STRUCTURE: a simulation study. Mol. Ecol. 14, 2611–2620.

Fouquet, A., Green, D.M., Waldman, B., Bowsher, J.H., McBride, K.P., Gemmell, N.J., 2010. Phylogeography of *Leiopelma hochstetteri* reveals strong genetic structure and suggests new conservation priorities. Conserv. Genet. 11, 907–919.

Garrick, R.C., Sunnucks, P., Dyer, R.J., 2010. Nuclear gene phylogeography using PHASE: dealing with unresolved genotypes, lost alleles, and systematic bias in parameter estimation. BMC Evol. Biol. 10, 118.

Hey, J., 2010. Isolation with migration models for more than two populations. Mol. Biol. Evol. 27, 905–920.

Hey, J., Nielsen, R., 2004. Multilocus methods for estimating population sizes, migration rates and divergence time, with applications to the divergence of *Drosophila pseudoobscura* and *D. persimilis*. Genetics 167, 747–760.

Hurt, C., Silliman, K., Anker, A., Knowlton, N., 2013. Ecological speciation in anemone-associated snapping shrimps (*Alpheus armatus* species complex). Mol. Ecol. 22, 4532–4548.

Igawa, T., Kurabayashi, A., Nishioka, M., Sumida, M., 2006. Molecular phylogenetic relationship of toads distributed in the Far East and Europe inferred from the nucleotide sequences of mitochondrial DNA genes. Mol. Phylogenet. Evol. 38, 250–260.

492 Iijima, A., Tada, R., 1990. Evolution of tertiary sedimentary basins of Japan in reference to
493 opening of the Japan Sea. J. Fac. Sci. Univ. Tokyo, Sect. II 22, 121–171.
494 Jacobsen, F., Omland, K.E., 2012. Extensive introgressive hybridization within the northern
495 oriole group (Genus *Icterus*) revealed by three-species isolation with migration analysis.
496 Ecol. Evol. 2, 2413–2429.
497 Jobb, G., 2011. TREEFINDER version March 2011. <http://www.treefinder.de>.
498 Kusano, T., Fukuyama, K., Miyashita, N., 1995a. Age determination of the stream frog, *Rana*
499 *sakuraii*, by skeletochronology. J. Herpetol. 29, 625–628.
500 Kusano, T., Fukuyama, K., Miyashita, N., 1995b. Body size and age determination brown frog
501 *Rana tagoi tagoi* by skeletochronology in southwestern Kanto. Jpn. J. Herpetol. 16, 29–34.
502 Lawson, L.P., 2010. The discordance of diversification: evolution in the tropical-montane frogs
503 of the Eastern Arc Mountains of Tanzania. Mol. Ecol. 19, 4046–4060.
504 Macey, J.R., Schulte, J.A, Larson, A., Fang, Z., Wang, Y., Tuniyev, B.S., Papenfuss, T.J., 1998.
505 Phylogenetic relationships of toads in the *Bufo bufo* species group from the eastern
506 escarpment of the Tibetan Plateau: a case of vicariance and dispersal. Mol. Phylogenet.
507 Evol. 9, 80–87.
508 Macey, J.R., Strasburg, J.L., Brisson, J. a, Vredenburg, V.T., Jennings, M., Larson, A., 2001.
509 Molecular phylogenetics of western North American frogs of the *Rana boylii* species
510 group. Mol. Phylogenet. Evol. 19, 131–143.
511 Maeda, N., Matsui, M., 1999. Frogs and Toads of Japan, Revised Edition. Bun–ichi Sogo
512 Shuppan, Tokyo.
513 Matsui, M., 2011. On the brown frogs from the Ryukyu Archipelago, Japan, with descriptions
514 of two new species (Amphibia, Anura). Curr. Herpetol. 30, 111–128.
515 Matsui, M., Shimada, T., Ota, H., Tanaka-Ueno, T., 2005. Multiple invasions of the Ryukyu
516 Archipelago by Oriental frogs of the subgenus *Odorrana* with phylogenetic reassessment
517 of the related subgenera of the genus *Rana*. Mol. Phylogenet. Evol. 37, 733–742.

518 Matsui, T., Matsui, M., 1990. A new brown frog (genus *Rana*) from Honshu, Japan.
519 Herpetologica 46, 78–85.
520 Mitsui, Y., Setoguchi, H., 2012. Demographic histories of adaptively diverged riparian and non-
521 riparian species of *Ainsliaea* (Asteraceae) inferred from coalescent analyses using multiple.
522 BMC Evol. Biol. 12, 254.
523 Nielsen, R., Wakeley, J., 2001. Distinguishing migration from isolation: a Markov chain Monte
524 Carlo approach. Genetics 158, 885–896.
525 Pritchard, J., Stephens, M., Donnelly, P., 2000. Inference of population structure using
526 multilocus genotype data. Genetics 155, 945–959.
527 Rambaut, A., Drummond, A., 2009. Tracer version 1.5. <http://beast.bio.ed.ac.uk/Tracer>.
528 Reilly, S.B., Marks, S.B., Jennings, W.B., 2012. Defining evolutionary boundaries across
529 parapatric ecomorphs of Black Salamanders (*Aneides flavipunctatus*) with conservation
530 implications. Mol. Ecol. 21, 5745–5761.
531 Roelants, K., Gower, D.J., Wilkinson, M., Loader, S.P., Biju, S.D., Guillaume, K., Moriau, L.,
532 Bossuyt, F., 2007. Global patterns of diversification in the history of modern amphibians.
533 Proc. Natl. Acad. Sci. U. S. A. 104, 887–892.
534 Ronquist, F., Huelsenbeck, J.P., 2003. MrBayes 3: Bayesian phylogenetic inference under
535 mixed models. Bioinformatics 19, 1572–1574.
536 Rovito, S.M., 2010. Lineage divergence and speciation in the Web-toed Salamanders
537 (Plethodontidae: *Hydromantes*) of the Sierra Nevada, California. Mol. Ecol. 19, 4554–
538 4571.
539 Rozas, J., Sanchez-DelBarrio, J.C., Messeguer, X., Rozas, R., 2003. DnaSP, DNA
540 polymorphism analyses by the coalescent and other methods. Bioinformatics 19, 2496–
541 2497.
542 Stephens, M., Smith, N., Donnelly, P., 2001. A new statistical method for haplotype
543 reconstruction from population data. Am. J. Hum. Genet. 68, 978–989.

544 Tajima, F., 1989. Statistical method for testing the neutral mutation hypothesis by DNA
545 polymorphism. Genetics 123, 585–595.
546 Tanabe, A.S., 2011. Kakusan4 and Aminosan: two programs for comparing nonpartitioned,
547 proportional and separate models for combined molecular phylogenetic analyses of
548 multilocus sequence data. Mol. Ecol. Resour. 11, 914–921.
549 Tanaka, T., Matsui, M., Takenaka, O., 1996. Phylogenetic relationships of Japanese brown
550 frogs (*Rana*: Ranidae) assessed by mitochondrial cytochrome b gene sequences. Biochem.
551 Syst. Ecol. 24, 299–307.
552 Tanaka-Ueno, T., Matsui, M., Chen, S.-L., Takenaka, O., Ota, H., 1998. Phylogenetic
553 relationships of brown frogs from Taiwan and Japan assessed by mitochondrial
554 cytochrome b gene sequences (*Rana*: Ranidae). Zool. Sci. 15, 283–288.
555 Tavaré, S., 1986. Some probabilistic and statistical problems in the analysis of DNA sequences,
556 in: Miura, R.M. (Ed.), Lectures on Mathematics in the Life Sciences. pp. 57–86.
557 Waples, R., Gaggiotti, O., 2006. What is a population? An empirical evaluation of some genetic
558 methods for identifying the number of gene pools and their degree of connectivity. Mol.
559 Ecol. 15, 1419–1439.
560 Woerner, A.E., Cox, M.P., Hammer, M.F., 2007. Recombination-filtered genomic datasets by
561 information maximization. Bioinformatics 23, 1851–1853.
562 Wright, S., 1931. Evolution in Mendelian populations. Genetics 16, 97–159.
563

564 **Supporting information**

565 Additional supporting information may be found in the online version of this article.
566

Table Captions

Table 1 The mean estimated divergence times (MYA) for *R. tagoi*, *R. sakuraii*, and the outgroups. Values in parentheses are the 95% highest posterior density interval. For the node numbers, refer to Fig. 2.

Table 2 Demographic parameters estimated in the IM analysis. N_e, effective population size (million individuals); $2N_eM$, effective population migration rate (number of gene copies/generation), for which $2N_eM_{1\rightarrow2}$ ($2N_eM_{2\rightarrow1}$) indicates gene flow from group 1 to 2 (2 to 1) forwards in time; *T*, population divergence time (MYA). Values supported by the highest probability are shown as HiPt, and HPD95 indicates the 95% highest posterior density interval. Parameters in bold indicate the values with statistical support, and characters in italics are those with no significant peak of posterior probability density.

Figure Captions

Fig. 1 Map showing the sampling localities of *Rana tagoi tagoi* (circles), *R. t. yakushimensis* (double circle), *R. t. okiensis* (stars), and *R. sakuraii* (triangles). Each species lineage inferred using mitochondrial haplotypes is represented by different markers. For the locality information, see Table S1.

Fig. 2 Maximum-likelihood tree based on the complete mitochondrial *16S* and *ND1* sequences (2579 bp in total) for *Rana tagoi* and *R. sakuraii*. For the locality number, see Fig. 1. Haplotypes in Clades A' and B are sampled from Honshu or the Oki Island (B-1). Haplotypes in Clades A" are from Kyushu, Shikoku, or adjacent small islands.

Fig. 3 Results of STRUCTURE analyses based on the five nuclear genes. Each species lineage inferred using mitochondrial haplotypes is separated by black vertical lines. (top) The best

clustering result (K = 2 clusters) for all 128 samples. (left bottom) Results with K=2 (best) and 3 for Cluster I. (right bottom) Results with K=3 (best) and 4 for Cluster II.

Fig. **4** Hypothesized scenarios for non-monophyly of mitochondrial haplotypes in *R. sakuraii*: (1) the species-level ILS hypothesis; and (2) the past mitochondrial introgression hypothesis, in which introgression occurred from *R. tagoi* Lineage A-2 to *R. sakuraii* (a) or in the opposite direction (b). Solid and broken lines indicate the mitochondrial lineages of *R. tagoi* and *R. sakuraii*, respectively. Grey arrows indicate massive mitochondrial introgression.

Captions for supplementary materials

Table S1 The samples used in this study with information on the sampling localities, vouchers, and GenBank accession numbers for each locus. KUHE, Graduate School of Human and Environmental Studies, Kyoto University; TMP, temporary number.

Table S2 The primers used to amplify mt- and n-DNA in this study.

Table S3 Summary statistics of each locus. Tajima's *D* values; length of sequence after alignment; variable sites (*vs*); number of haplotypes (*h*); haplotype diversity (*Hd*); and nucleotide diversity (π).

Fig. **S1** Median-joining networks of five nuclear loci. The size of each circle reflects the relative sample size of each haplotype. The color indicates nuclear clusters and species as follows: red = n-Cluster I of *R. tagoi*; green = n-Cluster II of *R. tagoi*; light green = n-Cluster II of *R. sakuraii*. Black circles and bars indicate median vectors and missing haplotypes, respectively.

618 **Fig**. **S2** Posterior probability densities for divergence time (*T*), effective population size (N_e),
619 and population migration rate ($2N_eM$) of Clusters I and II obtained in the IM analyses. The
620 resultant values and 95% confidence intervals for each estimate are listed in Table 2.
621
622 **Fig**. **S3** Posterior probability densities for divergence time (*T*, left top), effective population size
623 (N_e, left middle and bottom), and population migration rate ($2N_eM$, right) of *R. tagoi* (*Rt*)
624 lineage A-2, A-5+6, and *R. sakuraii* (*Rs*). Estimates with no statistical support are indicated by
625 *ns*. The parameters obtained in three- and two-populations models are shown as triangles and
626 circles, respectively. The resultant values and 95% confidence intervals for each estimate are
627 listed in Table 2.
628
629
630 The English in this document has been checked by at least two professional editors, both native
631 speakers of English. For a certificate, please see:
632 http://www.textcheck.com/
633 certificate/wc1m0N
634

Table 1 The mean estimated divergence times (MYA) for *R. tagoi* , *R. sakuraii* , and the outgroups. Values in parentheses are the 95% highest posterior density interval. For the node numbers, refer to Fig.

Node	Calibration I	Calibration II
1	4.00 (5.96–2.33)	4.16 (6.16–2.44)
2	2.58 (3.82–1.60)	2.82 (4.07–1.69)
3	2.31 (3.38–1.42)	2.46 (3.54–1.45)
4	1.84 (2.69–1.05)	1.73 (2.60–0.99)
5	1.16 (1.87–0.60)	1.04 (1.66–0.50)
6	1.32 (2.00–0.69)	1.35 (2.06–0.70)
7	1.87 (2.78–1.05)	2.08 (3.07–1.21)
8	0.95 (1.60–0.44)	1.13 (1.78–0.58)
9	0.88 (1.40–0.41)	1.39 (2.16–0.72)
10	1.92 (2.85–1.09)	2.12 (3.14–1.24)
11	1.75 (2.59–0.96)	1.69 (2.50–0.90)
12	0.50 (0.95–0.14)	0.42 (0.81–0.11)
13	1.15 (1.85–0.56)	1.50 (2.30–0.82)
14	0.36 (0.64–0.13)	0.53 (0.90–0.21)
15	2.31 (3.36–1.34)	2.54 (3.70–1.53)
16	0.79 (1.30–0.34)	0.85 (1.38–0.37)
17	0.20 (0.43–0.03)	0.17 (0.37–0.01)
18	1.68 (2.53–0.99)	1.98 (2.91–1.19)
19	0.53 (0.90–0.21)	0.59 (1.01–0.24)
20	1.04 (1.67–0.46)	1.40 (2.11–0.73)
21	1.46 (2.22–0.76)	1.54 (2.34–0.83)
22	2.71 (4.34–1.40)	2.29 (3.50–1.24)
23	1.40 (2.15–0.71)	1.35 (2.07–0.71)
24	0.80 (1.28–0.36)	0.82 (1.32–0.39)
25	0.90 (1.46–0.42)	1.08 (1.74–0.52)
26	0.04 (0.13–0.03)	0.26 (0.53–0.05)
O-1	22.02 (35.97–11.08)	11.59 (18.29–6.42)

Table 2 Demographic parameters estimated in the IM analysis. N_e, effective population size (million individuals); $2N_eM$, effective population migration rate (number of gene copies/generation), for which $2N_eM_{1\rightarrow2}$ ($2N_eM_{2\rightarrow1}$) indicates gene flow from group 1 to 2 (2 to 1) forwards in time; T, population divergence time (MYA). Values supported by the highest probability are shown as HiPt, and HPD95 indicates the 95% highest posterior density interval. Parameters in bold indicate the values with statistical support and characters in italics are those with no significant peak of posterior probability density.

	N_1	N_2	$N_{ancestor}$	$2N_eM_{1\rightarrow2}$	$2N_eM_{2\rightarrow1}$	T
(1) Cluster I vs. (2) Cluster II						
HiPt	2.18	1.73	0.40	**0.52**	**1.23**	2.72
HPD95	(1.70–2.87)	(1.34–2.30)	(0.17–0.79)	(0.24–1.12)	(0.70–2.14)	(2.10–4.29)
Three-pops. model: (1) *R. sakuraii* vs. (2) *R. tagoi* lin						
HiPt	0.16	0.80	0.21	0.01	0.00	1.05
HPD95	(0.07–0.32)	(0.34–2.06)	(0.01–4.06)	(0.00–2.46)	(0.00–0.84)	(0.63–2.26)
Three-pops. model: (1) *R. sakuraii* vs. (2) *R. tagoi* lineage A-5, 6						
HiPt	0.16	0.79	-	0.46	**0.40**	-
HPD95	(0.07–0.31)	(0.38–1.76)	-	(0.00–2.52)	(0.04–2.00)	-
Three-pops. model: (1) *R. tagoi* A-2 vs. (2) *R. tagoi* A-5, 6						
HiPt	0.80	0.79	-	0.17	**3.79**	-
HPD95	(0.34–2.06)	(0.38–1.76)	-	(0.00–3.74)	(0.75–9.50)	-
Three-pops. model: (1) ancestor of *R. sakuraii* and *R. tagoi* A-2 vs. (2) *R. tagoi* A-5, 6						
HiPt	0.21	0.79	0.43	*0.06*	*0.04*	2.15
HPD95	(0.01–4.06)	(0.38–1.76)	(0.23–0.77)	(0.00–81.15)	(0.00–34.07)	(1.31–6.11)
Two-pops. model: (1) *R. sakuraii* vs. (2) *R. tagoi* A-2, 5, 6						
HiPt	0.17	1.61	0.37	0.01	**0.51**	1.21
HPD95	(0.09–0.34)	(0.99–2.65)	(0.10–0.68)	(0.00–3.19)	(0.14–1.17)	(0.56–2.85)

Table S1 The samples used in this study with information on the sampling localities, vouchers, and GenBank accession numbers for each locus. KUHE, Graduate School of Human and Environmental Studies, Kyoto University; TMP, temporary number.

loc. nos.	locality	voucher (KUHE)	mt-lineage	GenBank accession no.					
				mtDNA (*16S* , *ND1*)	*NCX1*	*NFIA*	*POMC*	*SLC8A3*	*TYR*
Rana tagoi tagoi									
1	Mutsu City, Aomori Pref.	44827	A-1a	AB639413, AB639593	AB968741	AB968871	AB968996	AB969125	AB969253
2	Noshiro City, Akita Pref.	46598	A-1a	AB968306	AB968765	AB968894	AB969021	AB969150	AB969279
3	Ichinoseki City, Iwate Pref.	36699	A-1a	AB639413, AB639598	AB968687	AB968816	AB968942	AB969071	AB969199
4	Sendai City, Miyagi Pref.	45622	A-1a	AB968302	AB968761	AB968890	AB969017	AB969146	AB969274
5	Yamagata City, Yanagata Pref.	37543	A-1a	AB639417, AB639601	AB968689	AB968818	AB968944	AB969073	AB969201
6	Nihonmatsu City, Fukushima Pref.	29595	A-1a	AB639419, AB639604	AB968676	AB968805	AB968931	AB969060	AB969189
7	Nihonmatsu City, Fukushima Pref.	36330	A-2	AB639474, AB639643	AB968686	AB968815	AB968941	AB969070	AB969198
8	Daigo town, Ibaraki Pref.	42344	A-1a	AB639420, AB639605	AB968703	AB968832	AB968958	AB969087	AB969215
		43723	A-1a	AB968270	AB968725	AB968854	AB968980	AB969109	AB969237
		43886	A-2	AB639421, AB639646	AB968728	AB968857	AB968983	AB969112	AB969240
		TMP_081122-1	A-2	AB968251	AB968772	AB968784	AB969029	AB969156	AB969158
9	Tsukuba City, Ibaraki Pref.	42747	A-2	AB639479, AB639648	AB968709	AB968838	AB968964	AB969093	AB969221
10	Ichihara City, Chiba Pref.	28409	A-2	AB639482, AB639652	AB968673	AB968803	AB968929	AB969058	AB969186
		46172	A-2	AB968305	AB968764	AB968893	AB969020	AB969149	AB969277
11	Kanuma City, Tochigi Pref.	40166	A-1a	AB639422, AB639609	AB968690	AB968819	AB968945	AB969074	AB969202
12	Uonuma City, Nigata Pref.	36896	A-1a	AB639429, AB639612	AB968688	AB968817	AB968943	AB969072	AB969200
13	Nakanojo Town, Gunma Pref.	44810	A-1a	AB968281	AB968739	AB968869	AB968994	AB969123	AB969251
		44811	A-1a	AB968282	AB968740	AB968870	AB968995	AB969124	AB969252
		22930	A-4	AB639487, AB639657	AB968658	AB968787	AB968913	AB969042	AB969171
		22936	A-4	AB639487, AB639657	AB968659	AB968788	AB968914	AB969043	AB969172
		44797	A-4	AB968280	AB968738	AB968868	AB968993	AB969122	AB969250
14	Saku City, Nagano Pref.	43980	A-2	AB968274	AB968732	AB968861	AB968987	AB969116	AB969244
15	Akiruno City, Tokyo Pref.	42452	A-2	AB639483, AB639651	AB968705	AB968834	AB968960	AB969089	AB969217
		42453	A-2	AB968263	AB968706	AB968835	AB968961	AB969090	AB969218
16	Fujikawaguchiko Town, Yamanashi Pref.	45558	A-2	AB968300	AB968759	AB968888	AB969015	AB969144	AB969272
		43480	A-6	AB639493, AB639663	AB968716	AB968845	AB968971	AB969100	AB969228
17	Minobu Town, Yamanashi Pref.	45552	A-2	AB968299	AB968758	AB968887	AB969014	AB969143	AB969271
		45549	A-6	AB968298	AB968757	AB968886	AB969013	AB969142	AB969270
18	Izu City, Shizuoka Pref.	43468	A-2	AB639485, AB639655	AB968715	AB968844	AB968970	AB969099	AB969227
19	Hokuto City, Yamanashi Pref.	43483	A-5	AB639489, AB639659	AB968717	AB968846	AB968972	AB969101	AB969229
23	Nagano City, Nagano Pref.	18005	A-5	AB639488, AB639658	AB968654	AB968782	AB968909	AB969038	AB969167
24	Kurobe City, Toyama Pref.	45102	A-1a	AB968287	AB968746	AB968876	AB969002	AB969131	AB969259
		45103	A-1a	AB968288	AB968747	AB968877	AB969003	AB969132	AB969260
		45014	A-5	AB968283	AB968742	AB968872	AB968998	AB969127	AB969255
		45099	A-5	AB968286	AB968745	AB968875	AB969001	AB969130	AB969258
25	Takayama City, Gifu Pref.	42048	A-1a	AB968261	AB968700	AB968829	AB968955	AB969084	AB969212
		43018	A-1a	AB639434, AB639617	AB968711	AB968840	AB968966	AB969095	AB969223
26	Gujo City, Gifu Pref.	14228	A-5	AB639490, AB639660	AB968652	AB968780	AB969027	AB969036	AB969165
27	Fujieda City, Shizuoka Pref.	17955	A-6	AB639498, AB639668	AB968653	AB968781	AB968908	AB969037	AB969166
28	Neba Village, Nagano Pref.	27335	A-6	AB639500, AB639670	AB968665	AB968794	AB968920	AB969049	AB969178
		27337	A-6	AB968254	AB968666	AB968795	AB968921	AB969050	AB969179
29	Shinjo City, Aichi Pref.	45913	A-6	AB968304	AB968763	AB968892	AB969019	AB969148	AB969276
30	Okazaki City, Aichi Pref.	45910	A-6	AB968303	AB968762	AB968891	AB969018	AB969147	AB969275
31	Ise City, Mie Pref.	42829	A-6	AB639502, AB639672	AB968710	AB968839	AB968965	AB969094	AB969222
33	Ibigawa Town, Gifu Pref.	27388	A-1a	AB639436, AB639619	AB968667	AB968796	AB968922	AB969051	AB969180
34	Takashima City, Shiga Pref.	43925	A-1a	AB968273	AB968731	AB968860	AB968986	AB969115	AB969243
		43924	A-1b	AB968272	AB968730	AB968859	AB968985	AB969114	AB969242
35	Taga Town, Shiga Pref.	43512	B-2a	AB968266	AB968718	AB968847	AB968973	AB969102	AB969230
36	Matsuzaka City, Mie Pref.	41484	B-2a	AB639551, AB639716	AB968698	AB968827	AB968953	AB969082	AB969210
37	Joyo City, Kyoto Pref.	41554	B-2a	AB639549, AB639714	AB968699	AB968828	AB968954	AB969083	AB969211
38	Odai Town, Mie Pref.	40190	B-2a	AB639553, AB639718	AB968691	AB968820	AB968946	AB969075	AB969203
		45047	B-2a	AB968284	AB968743	AB968873	AB968999	AB969128	AB969257
39	Gobo City, Wakayama Pref.	41229	B-2a	AB639561, AB639727	AB968693	AB968822	AB968948	AB969077	AB969205
40	Kyoto City, Kyoto Pref.	42342	A-1b	AB968262	AB968702	AB968831	AB968957	AB969086	AB969214
		44828	A-1b	AB968307	AB968768	AB968896	AB968997	AB969126	AB969254
		42319	B-2a	AB639464, AB639712	AB968701	AB968830	AB968956	AB969085	AB969213
41	Nantan City, Kyoto Pref.	41408	A-1b	AB639452, AB639630	AB968695	AB968824	AB968950	AB969079	AB969207
		41405	B-2a	AB968259	AB968694	AB968823	AB968949	AB969078	AB969206
		41430	B-2a	AB968260	AB968697	AB968826	AB968952	AB969081	AB969209
42	Sasayama City, Hyogo Pref.	10307	A-1b	AB639469, AB639639	AB968647	AB968776	AB968903	AB969031	AB969160
43	Kobe City, Hyogo Pref.	45392	A-1b	AB968297	AB968756	AB968885	AB969012	AB969141	AB969269
44	Taka Town, Hyogo Pref.	10330	B-2a	AB639564, AB639729	AB968648	AB968777	AB968904	AB969032	AB969161
45	Kyotango City, Kyoto Pref.	14171	A-1b	AB968253	AB968651	AB968779	AB968907	AB969035	AB969164
46	Toyooka City, Hyogo Pref.	42711	A-1b	AB639466, AB639637	AB968707	AB968836	AB968962	AB969091	AB969219
		42714	B-2a	AB639467, AB639729	AB968708	AB968837	AB968963	AB969092	AB969220
47	Wakasa Town, Tottori Pref.	34743	A-1b	AB639473, AB639642	AB968684	AB968813	AB968939	AB969068	AB969196
49	Mimasaka City, Okayama Pref.	27659	B-2a	AB639464, AB639730	AB968670	AB968800	AB968926	AB969055	AB969183
52	Misasa Town, Tottori Pref.	24574	B-2b	AB639465, AB639731	AB968660	AB968789	AB968915	AB969044	AB969173
53	Kagamino Town, Okayama Pref.	29739	B-2b	AB968256	AB968677	AB968806	AB968932	AB969061	AB969190
54	Shobara City, Hiroshima Pref.	36040	B-2b	AB639469, AB639734	AB968685	AB968814	AB968940	AB969069	AB969197
55	Izumo City, Shimane Pref.	18877	B-2b	AB639467, AB639734	AB968655	AB968783	AB968910	AB969039	AB969168
57	Higashihiroshima City, Hiroshima Pref.	30262	B-2b	AB639472, AB639737	AB968678	AB968807	AB968933	AB969062	AB969191
58	Hatsukaichi City, Hiroshima Pref.	unnumbered	B-2b	AB639571, AB639736	AB968773	AB968901	AB969028	AB969157	AB969281
		43167	B-2b	AB968265	AB968713	AB968842	AB968968	AB969097	AB969225
60	Shimonoseki City, Yamaguchi Pref.	34516	B-2b	AB639575, AB639740	AB968682	AB968811	AB968937	AB969066	AB969278
61	Minamiawaji City, Hyogo Pref.	43885	A-7	AB639504, AB639673	AB968727	AB968856	AB968982	AB969111	AB969239
62	Manno Town, Kagawa Pref.	TMP_T2882	A-7	AB639505, AB639674	AB968770	AB968898	AB969024	AB969153	AB969283
63	Miyoshi City, Tokushima Pref.	TMP_T3498	A-7	AB968308	AB968771	AB968899	AB969025	AB969154	AB969284

64 Toyo Town, Kochi Pref.	29464	A-7	AB639510, AB639679	AB968675	AB968804	AB968930	AB969059	AB969188
65 Saijo City, Ehime Pref.	27679	A-7	AB639507, AB639676	AB968672	AB968802	AB968928	AB969057	AB969185
	43078	A-7	AB968264	AB968712	AB968841	AB968967	AB969096	AB969224
66 Saiyo City, Ehime Pref.	TMP_T2241	A-7	AB639509, AB639678	AB968769	AB968897	AB969023	AB969152	AB969282
67 Kitakyushu City, Fukuoka Pref.	28612	A-9a	AB968255	AB968674	AB968798	AB968924	AB969053	AB969187
68 Beppu City, Oita Pref.	43637	A-9a	AB639519, AB639688	AB968723	AB968852	AB968978	AB969107	AB969235
69 Yatsushiro City, Kumamoto Pref.	27562	A-9a	AB639524, AB639691	AB968668	AB968797	AB968923	AB969052	AB969181
70 Amakusa City, Kumamoto Pref.	30342	A-9a	AB639525, AB639692	AB968679	AB968808	AB968934	AB969063	AB969192
71 Kanoya City, Kagishima Pref.	27295	A-9a	AB639530, AB639697	AB968664	AB968793	AB968919	AB969048	AB969177
72 Sasebo City, Nagasaki Pref.	27140	A-9a	AB639518, AB639687	AB968663	AB968792	AB968918	AB969047	AB969176
73 Goto City, Nagasaki Pref.	45359	A-9a	AB968295	AB968754	AB968883	AB969010	AB969139	AB969267
	45362	A-9a	AB968296	AB968755	AB968884	AB969011	AB969140	AB969268
74 Nobeoka City, Miyazaki Pref.	27121	A-9b	AB639528, AB639695	AB968662	AB968791	AB968917	AB969046	AB969175
75 Nishimera Village, Miyazaki Pref.	26088	A-9b	AB639529, AB639696	AB968661	AB968790	AB968916	AB969045	AB969174
76 Miyakonojo City, Miyazaki Pref.	30907	A-9b	AB639532, AB639699	AB968680	AB968809	AB968935	AB969064	AB969193
77 Kimotsuki City, Kagoshima Pref.	43397	A-9b	AB639533, AB639700	AB968714	AB968843	AB968969	AB969098	AB969226
78 Kinko Town, Kagoshima Pref.	27678	A-9b	AB639536, AB639703	AB968671	AB968801	AB968927	AB969056	AB969184
79 Goto City, Nagasaki Pref.	31539	A-9c	AB639538, AB639705	AB968681	AB968810	AB968936	AB969065	AB969194
79 Shinkamigoto City, Nagasaki Pref.	45149	A-9c	AB968291	AB968750	AB968879	AB969006	AB969135	AB969263
	TMP_110216-1	A-9c	AB968252	AB968650	AB968774	AB968906	AB969034	AB969163
80 Goto City, Nagasaki Pref.	44316	A-9c	AB968278	AB968736	AB968866	AB968991	AB969120	AB969248
	44317	A-9c	AB968279	AB968737	AB968867	AB968992	AB969121	AB969249
	45355	A-9c	AB968294	AB968753	AB968882	AB969009	AB969138	AB969266
R. t. okiensis								
50 Okinoshima Town, Shimane Pref.	10818	B-1	AB639576, AB639742	AB968649	AB968778	AB968905	AB969033	AB969162
	22341	B-1	AB639579, AB639742	AB968656	AB968785	AB968911	AB969040	AB969169
51 Nishinoshima Town, Shimane Pref.	43647	B-1	AB639580, AB639742	AB968724	AB968853	AB968979	AB969108	AB969236
R. t. yakushimensis								
81 Yakushima Town, Kagoshima Pref.	10182	A-8	AB639578, AB639741	AB968646	AB968775	AB968902	AB969030	AB969159
	45177	A-8	AB968292	AB968751	AB968880	AB969007	AB969136	AB969264
	45182	A-8	AB968293	AB968752	AB968881	AB969008	AB969137	AB969265
R. sakuraii								
11 Kanuma City, Tochigi Pref.	43633	A-2	AB968268	AB968720	AB968849	AB968975	AB969104	AB969232
	43634	A-2	AB968269	AB968721	AB968850	AB968976	AB969105	AB969233
	43635	A-2	AB639423, AB639744	AB968722	AB968851	AB968977	AB969106	AB969234
15 Akiruno City, Tokyo Pref.	42450	A-2	AB639583, AB639744	AB968704	AB968833	AB968959	AB969088	AB969216
	43740	A-2	AB968271	AB968726	AB968855	AB968981	AB969110	AB969238
17 Minobu Town, Yamanashi Pref.	45620	A-2	AB968301	AB968760	AB968889	AB969016	AB969145	AB969273
20 Shizuoka City, Shizuoka Pref.	unnumbered	A-2	AB639488, AB639749	AB968766	AB968900	AB969022	AB969151	AB969280
	44254	A-3	AB968275	AB968733	AB968862	AB968988	AB969117	AB969246
	44286	A-3	AB968277	AB968735	AB968865	AB968990	AB969119	AB969247
21 Shizuoka City, Shizuoka Pref.	44256	A-2	AB968276	AB968734	AB968863	AB968989	AB969118	AB969245
22 Matsumoto City, Nagano Pref.	22887	A-2	AB639585, AB639746	AB968657	AB968786	AB968912	AB969041	AB969170
24 Kurobe City, Toyama Pref.	45105	A-3	AB968289	AB968748	AB968878	AB969004	AB969133	AB969261
24 Kurobe City, Toyama Pref.	45106	A-3	AB968290	AB968749	AB968864	AB969005	AB969134	AB969262
32 Katsuyama City, Fukui Pref.	43591	A-3	AB968267	AB968719	AB968848	AB968974	AB969103	AB969231
38 Odai Town, Mie Pref.	27647	A-3	AB639554, AB639719	AB968669	AB968799	AB968925	AB969054	AB969182
	40309	A-3	AB639555, AB639720	AB968692	AB968821	AB968947	AB969076	AB969204
	45049	A-3	AB968285	AB968744	AB968874	AB969000	AB969129	AB969256
41 Nantan City, Kyoto Pref.	41412	A-3	AB639455, AB639632	AB968696	AB968825	AB968951	AB969080	AB969208
	unnumbered	A-3	AB639454, AB639631	AB968767	AB968895	AB969026	AB969155	AB969285
48 Wakasa Town, Tottori Pref.	34740	A-3	AB968257	AB968683	AB968812	AB968938	AB969067	AB969195
59 Iwakuni City, Yamaguchi Pref.	43893	A-3	AB639590, AB639750	AB968729	AB968858	AB968984	AB969113	AB969241
R. tsushimensis								
Tsushima City, Nagasaku Pref.	10606		AB639592, AB639752	-	-	-	-	-
R. kobai								
Amami City, Kagoshima Pref.	10051		AB685768	-	-	-	-	-
R. ulma								
Higashi Village, Okinawa Pref.	10056		AB685780	-	-	-	-	-
R. sauteri								
Chiayi County, Taiwan	6894		AB685767	-	-	-	-	-

Table S2 The primers used to amplify mt- and n-DNA in this study.

Target	Name	Sequence	Reference
16S	L1507	TACACACCGCCCGTCACCCTCTT	Shimada et al (2011)
	H1923	AAGTAGCTCGCTTAGTTTCGG	Shimada et al (2011)
	L1879	CGTACCTTTTGCATCATGGTC	Shimada et al (2011)
	H2315	TTCTTGTTACTAGTTCTAGCAT	Shimada et al (2011)
	L2188	AAAGTGGGCCTAAAAGCAGCCA	Matsui et al (2006)
	Wilkinson_6	CCCTCGTGATGCCGTTGATAC	Wilkinson et al (2002)
	16L1	CTGACCGTGCAAAGGTAGCGTAATCACT	Hedges (1994)
	16H1	CTCCGGTCTGAACTCAGATCACGTAGG	Hedges (1994)
ND1	L3032	CGACCTCGATGTTGGATCAGG	Shimada et al (2011)
	ND1_Htago	GRGCRTATTTGGAGTTTGARGCTCA	Eto et al (2012)
	ND1_Ltago	GACCTAAACCTCAGYATYCTATTTAT	Eto et al (2012)
	tMet_H	AGGAAGTACAAAGGGTTTTGATC	Shimada et al (2011)
NCX1	NCX1F	ACAACAGTRAGRATATGGAA	Shimada et al. (2011)
	NCX1R1	GCCATATCTCTCCTCGCTTCTTC	Eto et al (2013)
NFIA	NFIA-005_F	TTTGTCACATCAGGTGTTTT	This study
	NFIA-005_R	CTTGCCTTGGCTGCT	This study
POMC	POMC1	GAATGTATYAAAGMMTGCAAGATGGWCC	Wiens et al. (2005)
	POMC7	TGGCATTTTTGAAAAGAGTCAT	Smith et al. (2005)
SLC8A3	SCF_2F	CAAACACAGRGSAATTATGAT	Shimada et al (2011)
	SCF_2R	ATAATYCCAACTGARAACTC	Shimada et al (2011)
TYR	Tyr_L1	CCCCAGTGGGYRCCCARTTCCC	Kuraishi et al (2013)
	Tyr_H1	CCACCTTCTGGATTTCCCGTTC	Kuraishi et al (2013)

References

Eto, K., Matsui, M., Sugahara, T., 2013. Discordance between mitochondrial DNA genealogy and nuclear DNA genetic structure in the two morphotypes of *Rana tagoi tagoi* (Amphibia: Anura: Ranidae) in the Kinki Region, Japan. Zool. Sci. 30, 553–558.

Eto, K., Matsui, M., Sugahara, T., Tanaka-Ueno, T., 2012. Highly complex mitochondrial DNA genealogy in an endemic Japanese subterranean breeding brown frog *Rana tagoi* (Amphibia, Anura, Ranidae). Zool. Sci. 29, 662–671.

Kuraishi, N., Matsui, M., Hamidy, A., Belabut, D.M., Ahmad, N., Panha, S., Sudin, A., Yong, H.S., Jiang, J.-P., Ota, H., Thong, H.T., Nishikawa, K., 2013. Phylogenetic and taxonomic relationships of the *Polypedates leucomystax* complex (Amphibia). Zool. Scripta, 42, 54–70.

Matsui M, Shimada T, Liu W-.Z., Maryati, M., Khonsue, W., Orlov, N., 2006. Phylogenetic relationships of Oriental torrent frogs in the genus *Amolops* and its allies (Amphibia, Anura, Ranidae). Mol. Phylogenet. Evol. 38, 659–666.

Shimada, T., Matsui, M., Yambun, P., Sudin, A. 2011. A taxonomic study of Whitehead's torrent frog, *Meristogenys whiteheadi* , with descriptions of two new species (Amphibia: Ranidae). Zool. J. Linnean, Soc, 161, 157–183.

Smith, S.A., Stephens, P.R., Wiens, J., 2005. Replicate patterns of species richness, historical biogeography, and phylogeny in Holarctic treefrogs. Evolution, 59, 2433–2450.

Wiens, J., Fetzner, J.W. Jr, Parkinson, C.L., Reeder, T.W., 2005. Hylid frog phylogeny and sampling strategies for species clades. Syst. Biol. 54, 719–748.

Wilkinson, J.A., Drewes, R.C., Tatum, O.L., 2002. A molecular phylogenetic analysis of the family Rhacophoridae with an emphasis on the Asian and African genera. Mol. Phylogenet. Evol. 24, 265–273.

Table S3 Summary statistics of each locus. Tajima's *D* values; length of sequence after alignment; variable sites (*vs*); number of haplotypes (*h*); haplotype diversity (*Hd*); and nucleotide diversity (π).

	Tajima's *D*	sites	*vs*	*h*	*Hd*	π	*vs*	*h*	*Hd*	π	*vs*	*h*	*Hd*	π	*vs*	*h*	*Hd*	π
	whole (n = 128)						mt-lineage A-1a (n = 18)				mt-lineage A-1b (n = 9)				mt-lineage A-2Rt (n = 12)			
16S	-1.307	1612	285	115	0.998	0.024	44	15	0.980	0.006	50	9	1.000	0.010	51	20	0.970	0.010
ND1	-0.816	967	287	104	0.997	0.047	44	14	0.974	0.010	70	9	1.000	0.026	53	10	0.970	0.016
NCX1 (*SLC8A1*)	-0.648	505	26	37	0.851	0.006	7	5	0.651	0.003	3	4	0.525	0.002	5	4	0.649	0.003
NFIA	-1.626	414	18	21	0.735	0.003	3	5	0.548	0.002	3	4	0.700	0.003	2	3	0.177	0.000
POMC	-1.538	475	40	48	0.870	0.007	9	6	0.712	0.004	7	6	0.775	0.004	12	10	0.859	0.006
SLC8A3 (*NCX3*)	-1.429	524	21	23	0.786	0.003	3	4	0.236	0.001	2	3	0.242	0.000	8	6	0.659	0.002
TYR	-1.210	318	50	97	0.955	0.017	17	12	0.867	0.013	15	12	0.958	0.018	20	15	0.946	0.018

	mt-lineage A-2*Rs* (n = 9)				mt-lineage A-3 (n = 12)				mt-lineage A-4 (n = 3)				mt-lineage A-5 (n = 5)			
16S	26	7	0.964	0.006	43	12	1.000	0.009	7	2	0.667	0.003	41	5	1.000	0.012
ND1	38	7	0.964	0.016	37	8	0.939	0.013	9	2	0.667	0.006	38	4	0.900	0.018
NCX1 (*SLC8A1*)	2	2	0.125	0.001	2	3	0.163	0.000	3	2	0.533	0.003	3	3	0.607	0.002
NFIA	1	2	0.125	0.000	2	3	0.163	0.000	2	3	0.600	0.002	1	2	0.250	0.001
POMC	6	5	0.556	0.003	9	5	0.652	0.004	3	2	0.533	0.003	4	3	0.607	0.003
SLC8A3 (*NCX3*)	1	2	0.125	0.000	2	3	0.554	0.001	1	2	0.533	0.001	1	2	0.571	0.001
TYR	11	4	0.442	0.008	9	5	0.493	0.007	1	2	0.533	0.002	12	7	0.964	0.018

	mt-lineage A-6 (n = 8)				mt-lineage A-7 (n = 7)				mt-lineage A-8 (n = 3)				mt-lineage A-9a (n = 8)			
16S	25	8	1.000	0.005	27	7	1.000	0.006	3	2	0.667	0.001	28	7	0.964	0.006
ND1	15	6	0.964	0.005	32	7	1.000	0.011	3	2	0.667	0.002	21	7	0.964	0.006
NCX1 (*SLC8A1*)	4	5	0.505	0.002	2	3	0.538	0.001	4	3	0.733	0.004	6	6	0.792	0.004
NFIA	2	3	0.425	0.001	2	3	0.275	0.001	2	3	0.600	0.002	2	3	0.433	0.001
POMC	9	7	0.850	0.006	-	1	-	-	4	3	0.600	0.003	2	3	0.242	0.001
SLC8A3 (*NCX3*)	2	2	0.363	0.001	2	2	0.440	0.002	-	1	-	-	1	2	0.264	0.001
TYR	16	13	0.975	0.016	9	7	0.846	0.009	10	4	0.800	0.013	11	7	0.692	0.009

	mt-lineage A-9b (n = 5)				mt-lineage A-9c (n = 6)				mt-lineage B-1 (n = 3)				mt-lineage B-2a (n = 12)			
16S	44	5	1.000	0.014	41	5	0.933	0.014	4	3	1.000	0.002	36	10	0.970	0.007
ND1	36	5	1.000	0.018	39	4	0.800	0.023	-	1	-	-	42	10	0.970	0.013
NCX1 (*SLC8A1*)	5	5	0.822	0.003	6	7	0.879	0.003	-	1	-	-	2	3	0.636	0.002
NFIA	2	2	0.200	0.001	4	5	0.756	0.004	1	2	0.333	0.001	1	2	0.228	0.001

POMC	6	3	0.378	0.003	7	5	0.742	0.006	8	5	0.933	0.008	9	7	0.851	0.004
SLC8A3 (*NCX3*)	3	4	0.644	0.001	-	1	-	-	3	4	0.867	0.003	4	5	0.361	0.002
TYR	12	9	0.978	0.013	11	6	0.848	0.014	6	5	0.933	0.009	10	9	0.812	0.010

	mt-lineage B-2b (n = 8)				n-cluster I (n = 68)				n-cluster II (n = 56)			
16S	24	7	0.964	0.006	204	61	0.996	0.026	176	53	0.997	0.018
ND1	33	7	0.964	0.014	218	57	0.994	0.049	192	47	0.994	0.037
NCX1 (*SLC8A1*)	7	6	0.833	0.005	19	26	0.875	0.005	12	13	0.483	0.002
NFIA	1	2	0.125	0.000	11	16	0.493	0.002	6	8	0.486	0.001
POMC	4	4	0.350	0.001	29	26	0.784	0.006	24	24	0.849	0.007
SLC8A3 (*NCX3*)	3	3	0.633	0.002	9	10	0.593	0.002	12	12	0.577	0.002
TYR	10	13	0.967	0.010	34	58	0.935	0.014	33	43	0.907	0.016

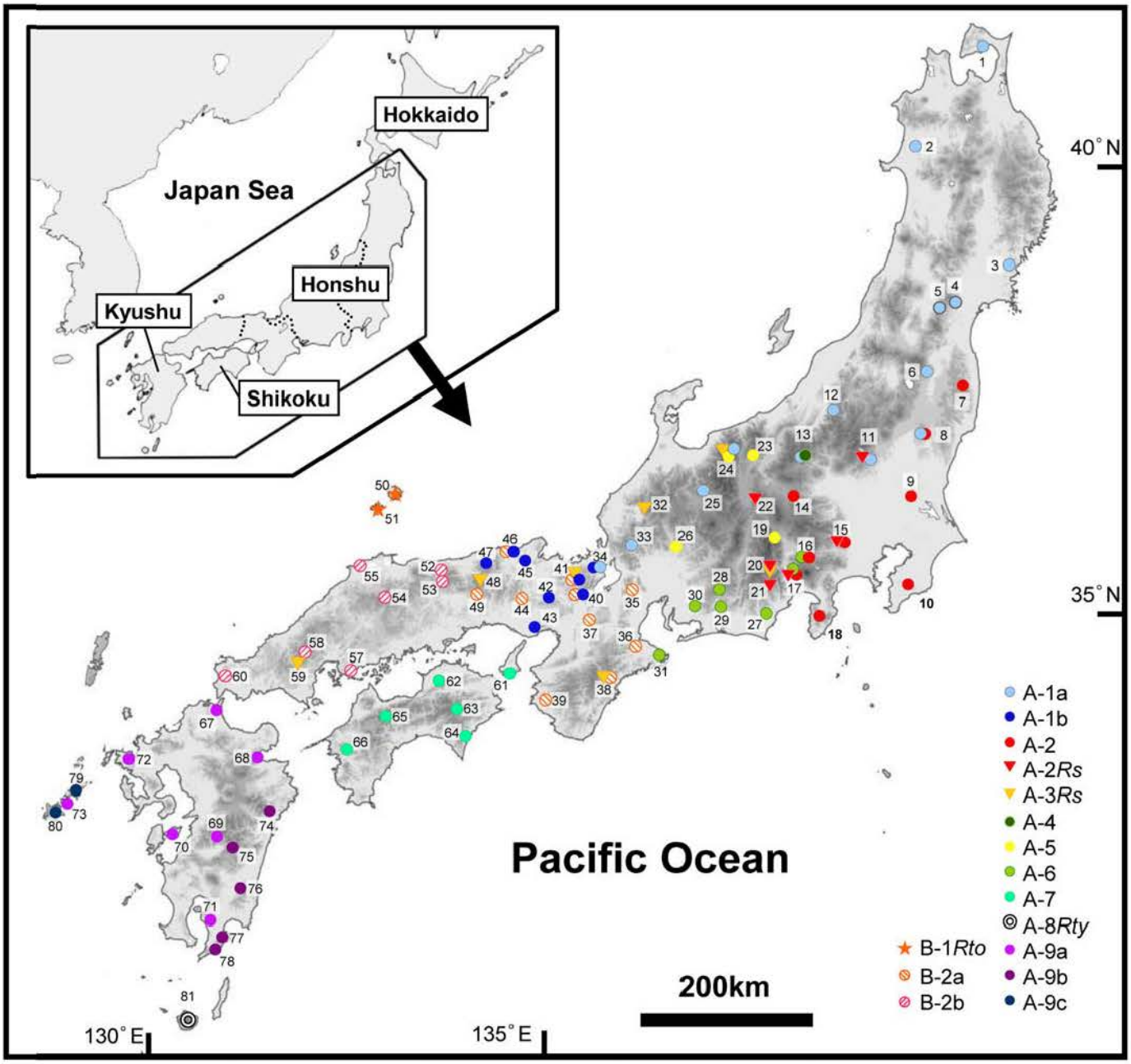

Fig. 1

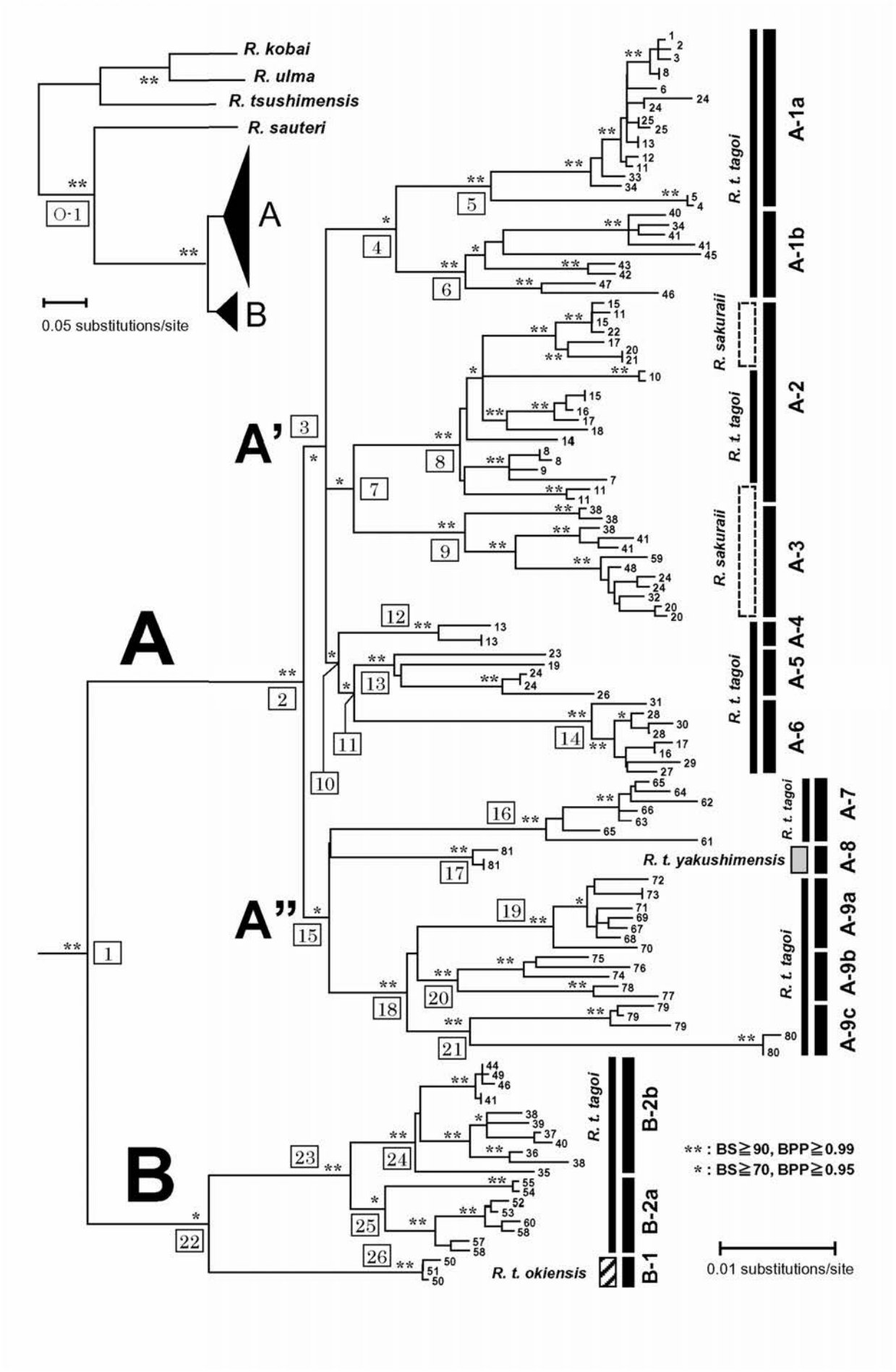

Fig. 2

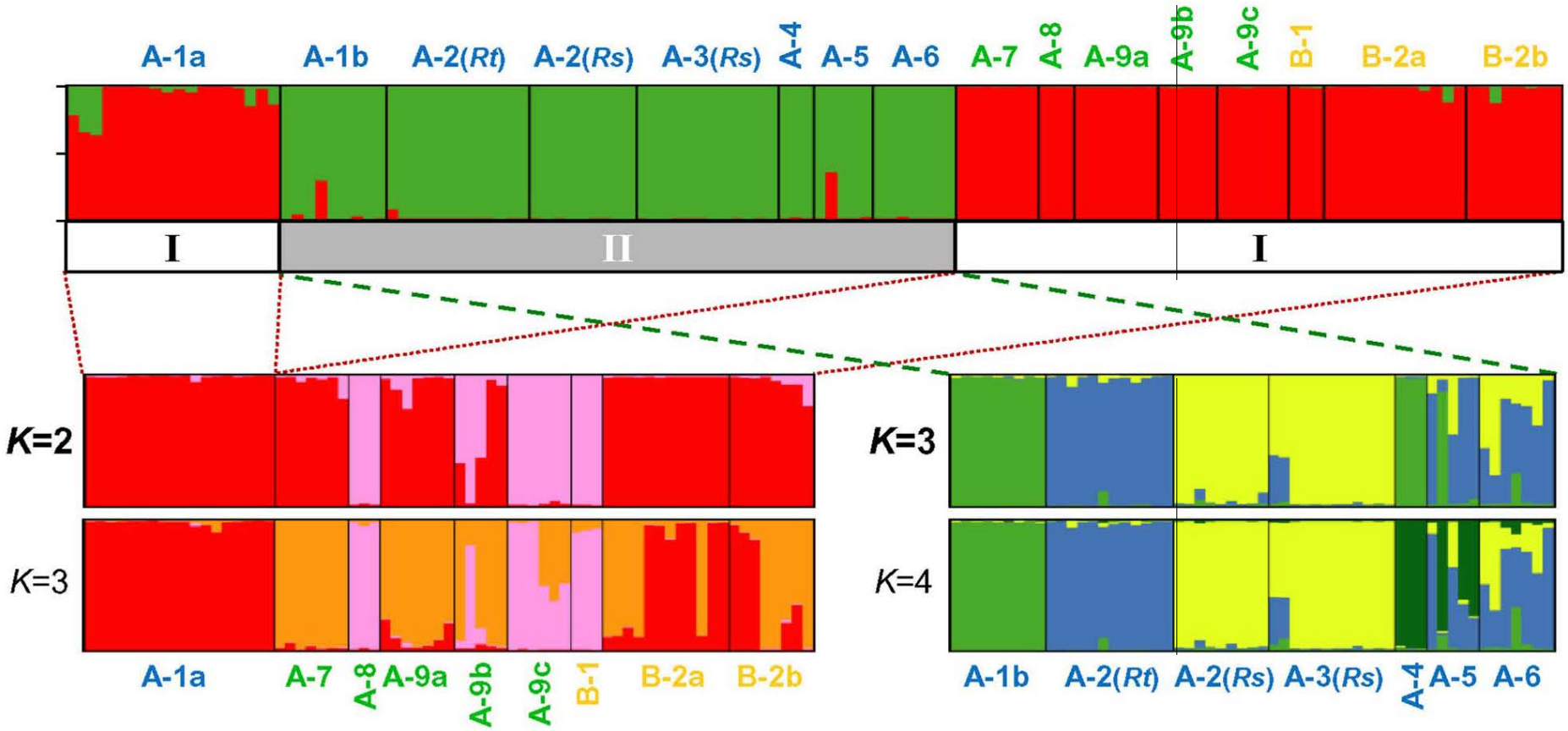
A-1a
A-1b
A-2(Rt)
A-2(Rs)
A-3(Rs)
A-4
A-5
A-6
A-7
A-8
A-9a
A-9b
A-9c
B-1
B-2a
B-2b
I
II
I
K=2
K=3
A-1a
A-7
A-8
A-9a
A-9b
A-9c
B-1
B-2a
B-2b
K=3
K=4
A-1b
A-2(Rt)
A-2(Rs)
A-3(Rs)
A-4
A-5
A-6

Fig. 3

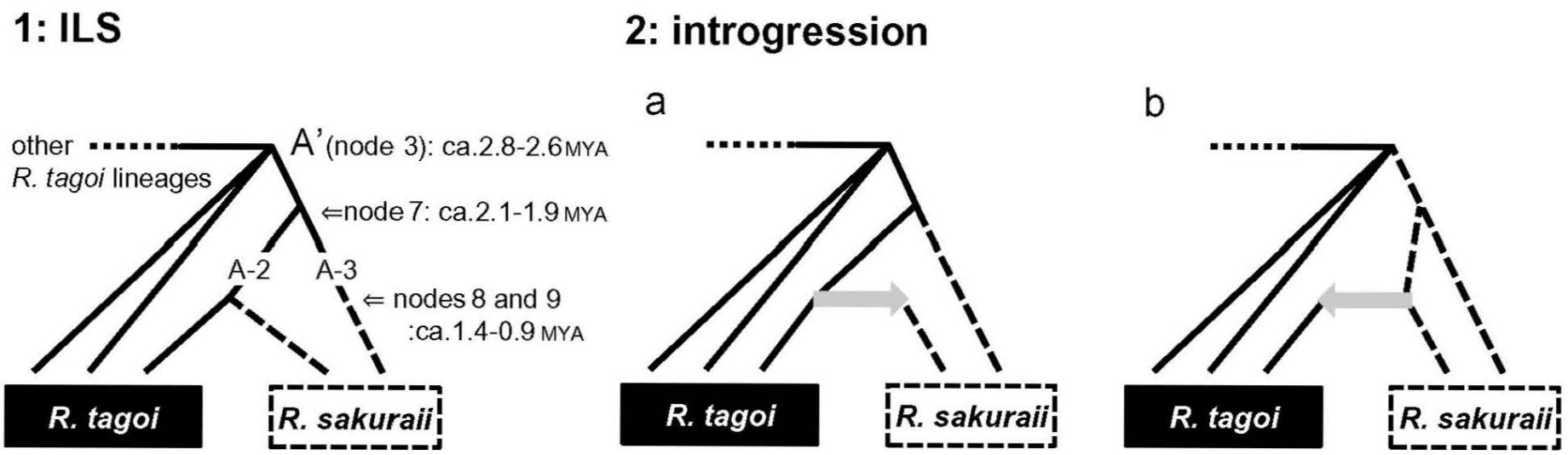

Fig. 4

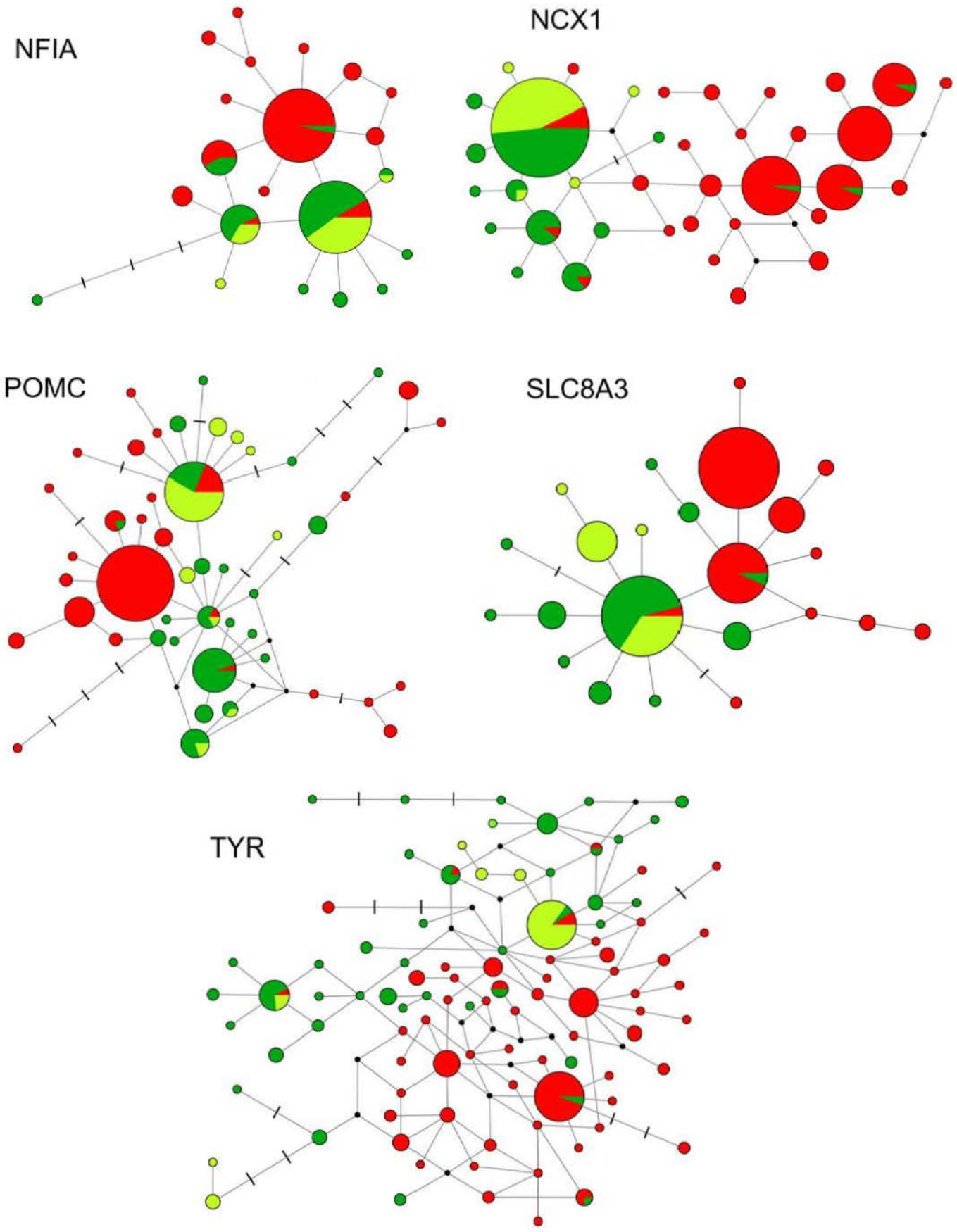

Fig. S1

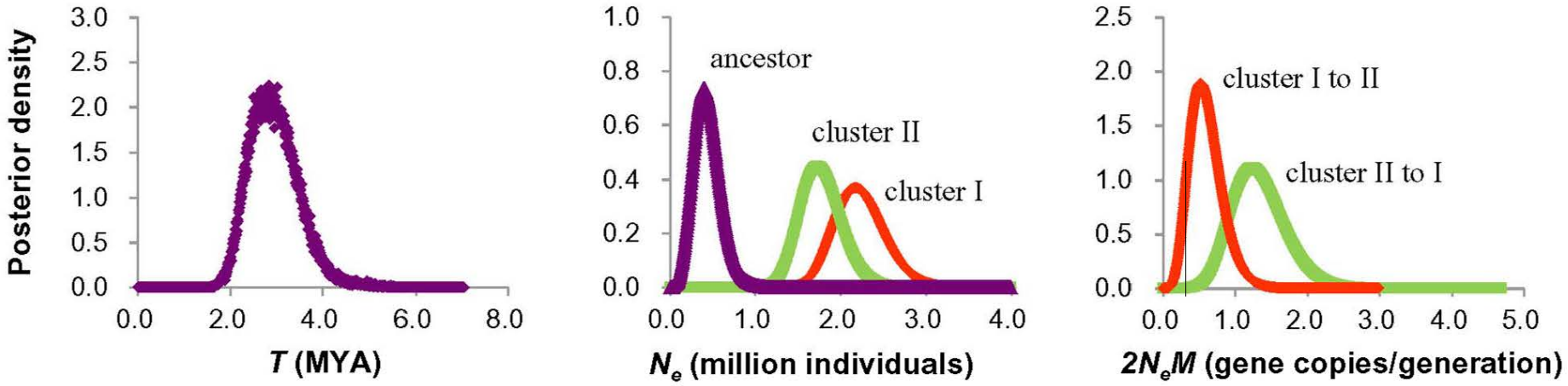
Posterior density
3.0
2.5
2.0
1.5
1.0
0.5
0.0
0.0
2.0
4.0
6.0
8.0
T (MYA)
1.0
0.8
0.6
0.4
0.2
0.0
ancestor
cluster II
cluster I
0.0
1.0
2.0
3.0
4.0
Ne (million individuals)
2.5
2.0
1.5
1.0
0.5
0.0
cluster I to II
cluster II to I
0.0
1.0
2.0
3.0
4.0
5.0
2NeM (gene copies/generation)

Fig. S2

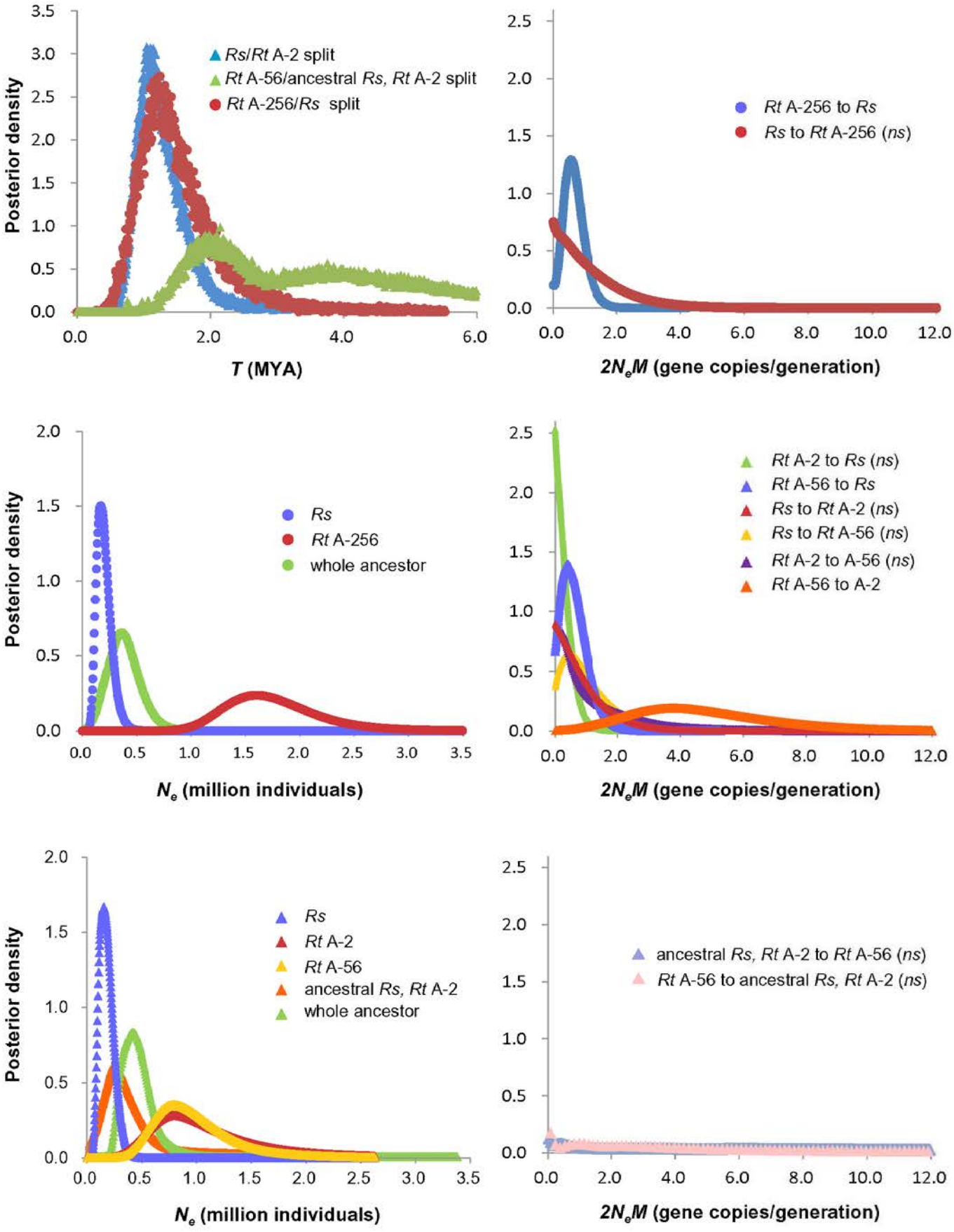

Fig. S3

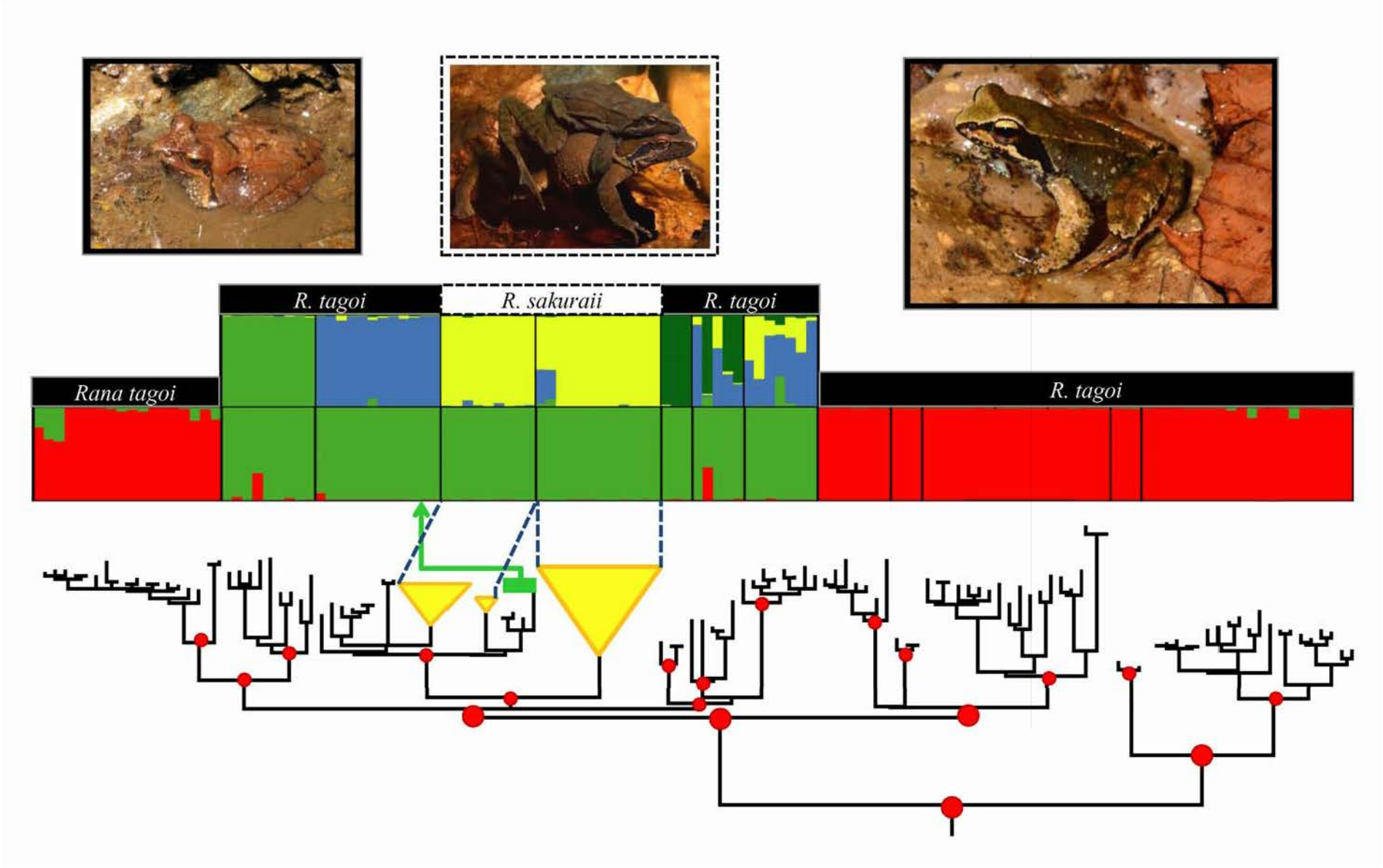

Graphical abstract